

Gravitational geons in asymptotically anti-de Sitter spacetimes

Grégoire Martinon¹

Gyula Fodor²

Philippe Grandclément¹

Peter Forgács^{2,3}

¹ LUTH, Observatoire de Paris, PSL Research University, CNRS, Université Paris Diderot, Sorbonne Paris Cité, 92190 Meudon, France

² Wigner Research Centre for Physics, RMKI, 1525 Budapest 114, P.O. Box 49, Hungary

³ LMPT, CNRS-UMR 6083, Université de Tours, Parc de Grandmont, 37200 Tours, France

E-mail: gregoire.martinon@obspm.fr

Abstract. We report on numerical constructions of fully non-linear geons in asymptotically anti-de Sitter (AdS) spacetimes in four dimensions. Our approach is based on 3+1 formalism and spectral methods in a gauge combining maximal slicing and spatial harmonic coordinates. We are able to construct several families of geons seeded by different families of spherical harmonics. We can reach unprecedentedly high amplitudes, with mass of order $\sim 1/2$ of the AdS length, and with deviations of the order of 50% compared to third order perturbative approaches. The consistency of our results with numerical resolution is carefully checked and we give extensive precision monitoring techniques. All global quantities like mass and angular momentum are computed using two independent frameworks that agree each other at the 0.1% level. We also provide strong evidence for the existence of excited (i.e. with one radial node) geon solutions of Einstein equations in asymptotically AdS spacetimes by constructing them numerically.

PACS numbers: 04.20.Cv, 04.20.Ex, 04.20.Ha, 04.25.D-, 04.25.Nx, 04.40.Nr, 11.25.Tq

Submitted to: *Class. Quantum Grav.*

Keywords: Geons, anti-de Sitter instability, Einstein equations, 3+1 formalism

1. Introduction

AdS spacetime has drawn a great deal of attention since the emergence of gauge/gravity duality [1–4], which basically states that string theory in asymptotically AdS spacetimes is equivalent to a conformal field theory (CFT) living on the AdS timelike boundary. The non-linear stability of the AdS spacetime is far from being settled and is of great interest.

In the seminal paper [5], the time-evolution of a free, massless scalar field coupled to Einstein’s gravity has been investigated in asymptotically AdS spacetimes. The authors found that for a large set of smooth initial data black holes form, indicating that AdS is unstable against black hole formation. It has been conjectured that no matter how small perturbation one considers in asymptotically AdS, it will eventually lead to the formation of a black hole. Various analytical studies and numerical experiments followed [6–26], accumulating more and more indications to the conjectured instability. Since asymptotically AdS spacetimes have timelike boundaries, by imposing energy-conserving boundary conditions, outgoing waves will bounce back from spatial infinity and reach the origin in finite time. The heuristic explanation for the instability of asymptotically AdS spacetimes is that by bouncing from the boundary many times, the waves concentrate more and more energy to smaller and smaller scales, leading to the formation of a black hole in a timescale proportional to the inverse square of the initial amplitude.

In a number of papers [27–29] it has been found that a real massless scalar field minimally coupled to gravity admits asymptotically AdS globally regular, spherically symmetric, time-periodic solutions, whose mass is finite. The existence of families of localized, time-periodic asymptotically AdS solutions (referred to as scalar AdS breathers) is intimately linked to the boundary conditions. In asymptotically flat spacetimes, breathers represent the exception to the rule “anything that can radiate, does radiate”, and they exist only in rather special circumstances (e.g. sine-Gordon theory in 1+1 dimension, scalar theories with V-shaped [30, 31] or logarithmic potentials [32]). On the other hand, families of long-lived, closely time-periodic *oscillons* exist in a number of field theories containing massive scalars in Minkowski or asymptotically flat spacetimes [33–35]. Oscillons emit energy very slowly, accompanied by a slow change of their amplitude and frequency [36–38]. It has been shown that the energy emission rate of small-amplitude oscillons is exponentially small in terms of a parameter corresponding to the central amplitude [39–41]. Flat background oscillons only exist for massive fields, since their frequency at small amplitude is determined by the scalar field mass. Massive scalar fields coupled to Einstein’s gravity also form long living, oscillating localized objects, referred to as *oscillatons* [42–44]. The mass loss rate of oscillatons can be extremely small even on cosmological time scales [45, 46]. Importantly oscillons/oscillatons form from generic initial data and are stable under time evolution.

Many years ago J. A. Wheeler introduced the concept of *geon*, a hypothetical, time-dependent solution of either Einstein or Einstein-Maxwell equations. The gravitational

geon would consist of high frequency gravitational waves, trapped in a background geometry created by the waves themselves *for much longer times* than the light crossing time [47]. We refer to [48, 49] for approximation procedures of gravitational geon in asymptotically flat space-times using frequency averaging and self-consistent methods. A theorem by G.W. Gibbons and J.M. Stuart [50] has established the absence of asymptotically flat solutions of Einstein equations which are time-periodic and empty near infinity, implying that if geons exist, they cannot be time-periodic i.e. they should necessarily radiate. This does not exclude the possibility that asymptotically flat geons would loose their mass slowly similarly to what has been found for oscillons/oscillatons.

The simplest and mostly investigated scalar AdS breathers are spherically symmetric and importantly some of them appear to be actually stable against collapsing to a black hole [27–29, 51–55]. A key ingredient for the construction of such solutions seems to be a large concentration of the energy into one single scalar eigenmode. The existence of such stable breathers indicate the presence of stability islands in asymptotically AdS spacetimes, likely forming sets of non-zero measure initial data.

In [56], it has been shown by a series expansion of the metric tensor that time-periodic solutions of Einstein’s equation with a negative cosmological constant, “gravitational AdS breathers”, or AdS *geons* are likely to exist. The perturbative expansion becomes inconsistent at third order, with the outbreak of a secular resonance. However, a standard Poincaré-Lindstedt method, which consist in promoting the geon frequency to a function of the amplitude, can be applied to cure this inconsistency, at least in some cases [57–59]. This suggests that fully non-linear geons can be constructed, and numerical solutions of the simplest family of geons were constructed in [60]. Geons can be seen as non-linear purely gravitational eigenmodes of asymptotically AdS spacetimes, being the fundamental excitations resisting the collapse to a black hole. They are among the key ingredients to better understand the AdS instability problem.

The main results of the present paper are the followings. (i) we give an independent construction of the fully non-linear $(l, m, n) = (2, 2, 0)$ geons that were constructed solely in [60]. Our results on global quantities disagree, to a certain extent, with this work, but strongly supported by convergent analytical and numerical arguments (section 7). (ii) we present the so-called Andersson-Moncrief gauge and discuss its theoretical motivations as well as its numerical implementation. We also make clear the link between this gauge and the harmonic gauge enforced with the popular De-Turck method (section 3 and appendix Appendix A). (iii) we extend the numerical constructions of fully non-linear geons to the $(l, m, n) = (4, 4, 0)$ case, as well as to the three excited families exhibiting one radial node. The existence of these excited geons was denied in [57], but supported in [58, 59] with perturbative arguments. Our results clearly provide evidence in favour of the existence of such solutions.

This paper is organised as follows. We carry out first a perturbative expansion around the AdS metric to construct approximations to AdS geons. Our perturbative approach is based on the Kodama-Ishibashi formalism [61–64], which method also has been used in [56]. Several AdS geon families are constructed, corresponding to the

quantum numbers $(l, m, n) = (2, 2, 0)$ and $(4, 4, 0)$ as well as all three radially excited families with $m = 2$. Then we present in detail our numerical construction of several different geon families, corresponding to different angular and radial excitations. As an initial guess, we use perturbative results, summarized in Section 2. In Section 3 we present a novel approach inspired by Andersson and Moncrief [65] and based on a 3+1 decomposition of Einstein equations [66] in a gauge combining maximal slicing and spacial harmonic coordinates. Section 4 is dedicated to our regularization procedure, as all fields in AdS are diverging. Section 5 is devoted to the definition of AdS asymptotics. In Section 6, we describe the numerical algorithm based on the Kadath spectral library [67]. In order to check the validity of our solutions, we build up an efficient precision monitoring. We then develop several diagnostics to check the precision of our code, in particular we ensure that our Dirichlet boundary conditions preserve the AdS asymptotics, in the sense of [68, 69]. Finally in Section 7, we build numerical geons at unprecedentedly high amplitudes, with deviations as high as 50% relative to third order perturbative approaches. We carefully extract global variables with two different methods, namely the Ashtekar-Magnon-Das (AMD) [68, 69] and the Balasubramanian-Kraus (BK) [70] that agree each other at the 0.1% level. We recover in the low amplitude limit the perturbative results up to fifth order, and give predictions about coefficients appearing at successive orders. Last but not least, we provide numerical evidence that radially excited geons, whose existence was debated in [57–59], do exist in AdS spacetimes. We compute them numerically and finally show their existence curves in phase space.

2. Perturbative approach

We denote by \bar{g} the 4-dimensional AdS metric. Following [61–64], we introduce coordinates that make the rotational invariance of the background explicit, namely

$$d\bar{s}^2 = \bar{g}_{\alpha\beta} dx^\alpha dx^\beta = \hat{g}_{ab}(y) dy^a dy^b + r^2(y) \tilde{\gamma}_{ij}(z) dz^i dz^j \quad (1)$$

$$= \frac{L^2}{\cos^2 \bar{x}} \left[-d\bar{t}^2 + d\bar{x}^2 + \sin^2 \bar{x} (d\theta^2 + \sin^2 \theta d\varphi^2) \right], \quad (2)$$

where L is related to the cosmological constant Λ by $\Lambda = -3/L^2$, y^a coordinates span the time-radial plane and z^i the unit sphere \mathcal{S}^2 whose metric is $\tilde{\gamma}_{ij}$. By identification, we will denote in this section $r = L \tan \bar{x}$. We look for families of solutions of the vacuum Einstein equation with a negative cosmological constant in the following form:

$$g_{\alpha\beta} = \bar{g}_{\alpha\beta} + \sum_{k=1}^{\infty} \varepsilon^k h_{\alpha\beta}^{(k)}, \quad (3)$$

where ε is a small expansion parameter and k denotes the orders of approximation. We assume that at infinity

$$\lim_{\bar{x} \rightarrow \frac{\pi}{2}} \left[h_{\bar{t}\bar{t}}^{(k)} \left(\frac{\pi}{2} - \bar{x} \right)^2 \right] = -L^2 \nu_k, \quad (4a)$$

$$\lim_{\bar{x} \rightarrow \frac{\pi}{2}} \left[h_{\alpha\beta}^{(k)} \left(\frac{\pi}{2} - \bar{x} \right)^2 \right] = 0 \quad \text{for } \alpha \neq \bar{t} \text{ or } \beta \neq \bar{t}, \quad (4b)$$

where ν_k are constants, independent of the angular coordinates, and they are generally nonzero only for even k . Then the leading order behavior of the $g_{\bar{t}\bar{t}}$ metric component is ε dependent,

$$\lim_{\bar{x} \rightarrow \frac{\pi}{2}} \left[g_{\bar{t}\bar{t}} \left(\frac{\pi}{2} - \bar{x} \right)^2 \right] = -\nu, \quad \nu = L^2 \left(1 + \sum_{k=1}^{\infty} \varepsilon^k \nu_k \right). \quad (5)$$

The advantage of this setting is that (i) it maintains the AdS asymptotics (in the sense of [64, 68, 69] and Section 5 below) and (ii) the frequency $\bar{\omega}$ of the geon can be kept independent of ε at all orders with respect to the time coordinate \bar{t} . The asymptotically AdS time coordinate is then $t = \bar{t}\sqrt{\nu}$, and the physical frequency of the solution is $\omega = \bar{\omega}/\sqrt{\nu}$.

At each order we decompose the metric perturbation $h_{\alpha\beta}^{(k)}$ into the sum of scalar and vector spherical harmonic components[‡], in the same way as it has been done for the linear case in [61, 64]. We choose a gauge in which scalar-type perturbations in the \mathbb{S}_{lm} real spherical harmonic class have the block diagonal form ($a, b = \bar{t}, \bar{x}$ and $i, j = \theta, \varphi$)

$$h_{ab}^{(k)} = H_{ab}^{(s)} \mathbb{S}, \quad h_{ai}^{(k)} = 0, \quad h_{ij}^{(k)} = H_L^{(s)} \tilde{\gamma}_{ij} \mathbb{S}, \quad (6)$$

and class $\mathbb{V}_{(lm)i}$ vector-type perturbations are

$$h_{ab}^{(k)} = 0, \quad h_{ai}^{(k)} = H_a^{(v)} \mathbb{V}_i, \quad h_{ij}^{(k)} = 0, \quad (7)$$

where we made implicit the (l, m) indices and the order k of the perturbation. Here the functions $H_{ab}^{(s)}$, $H_L^{(s)}$ and $H_a^{(v)}$ depend only on the coordinates $y^a = (\bar{t}, \bar{x})$. We use real spherical harmonics \mathbb{S}_{lm} that are orthonormal. The ϕ dependence of \mathbb{S}_{lm} for $m \geq 0$ is $\cos(m\phi)$, and for $m < 0$ it is $\sin(|m|\phi)$. The vector harmonics $\mathbb{V}_{(lm)i}$ can be expressed in terms of the scalar harmonics as

$$\mathbb{V}_{(lm)\theta} = \frac{1}{\sqrt{l(l+1)}} \frac{1}{\sin\theta} \frac{\partial \mathbb{S}_{lm}}{\partial \phi}, \quad \mathbb{V}_{(lm)\phi} = \frac{-1}{\sqrt{l(l+1)}} \sin\theta \frac{\partial \mathbb{S}_{lm}}{\partial \theta}. \quad (8)$$

Perturbative modes with $l \leq 1$ have to be treated separately. For the $l = 0$ scalar modes we further restrict the gauge by assuming $H_L^{(s)} = 0$ and $H_{\bar{t}\bar{x}}^{(s)} = 0$. For the $l = 1$ vector mode we set $H_{\bar{x}}^{(v)} = 0$.

For $l \geq 2$, the Kodama-Ishibashi-Seto [61] gauge-invariant variables Z , Z_a and Z_{ab} can be defined, and in our gauge they are related to the metric variables as

$$H_L^{(s)} = \frac{r^2}{2} Z, \quad H_{ab}^{(s)} = Z_{ab} - \frac{1}{2} Z g_{ab}^\circ, \quad H_a^{(v)} = Z_a. \quad (9)$$

In each scalar and vector class, perturbations are characterized by functions $\Phi^{(s)}$ and $\Phi^{(v)}$ respectively, satisfying the following master equation, deduced from the Einstein equation:

$$-\partial_{\bar{t}}^2 \Phi^{(s,v)} + \partial_{\bar{i}}^2 \bar{x} \Phi^{(s,v)} - \frac{l(l+1)}{\sin^2 \bar{x}} \Phi^{(s,v)} + \frac{\Phi^{(s,v)(0)}}{\sin^2 \bar{x}} = 0, \quad (10)$$

[‡] Tensor spherical harmonics appear only in spacetimes of dimension at least five.

where $\Phi^{(s,v)(0)}$ are inhomogeneous source terms fixed by lower order perturbations. The outer boundary conditions for the scalar and vector cases are respectively

$$\lim_{\bar{x} \rightarrow \frac{\pi}{2}} \partial_{\bar{x}} \Phi^{(s)} = 0 \quad \text{and} \quad \lim_{\bar{x} \rightarrow \frac{\pi}{2}} \Phi^{(v)} = 0. \quad (11)$$

From the scalar-type generating function, defining $\phi^{(s)} = r\Phi^{(s)}$, we obtain the gauge-invariant variables as

$$Z_{\bar{t}\bar{t}} = \partial_{\bar{t}}^2 \phi^{(s)} - \tan \bar{x} \partial_{\bar{x}} \phi^{(s)} + \frac{\phi^{(s)}}{\cos^2 \bar{x}} + Z_{\bar{t}\bar{t}}^{(0)}, \quad (12a)$$

$$Z_{\bar{t}\bar{x}} = \partial_{\bar{t}} \partial_{\bar{x}} \phi^{(s)} - \tan \bar{x} \partial_{\bar{t}} \phi^{(s)} + Z_{\bar{t}\bar{x}}^{(0)}, \quad (12b)$$

$$Z_{\bar{x}\bar{x}} = \partial_{\bar{x}}^2 \phi^{(s)} - \tan \bar{x} \partial_{\bar{x}} \phi^{(s)} - \frac{\phi^{(s)}}{\cos^2 \bar{x}} + Z_{\bar{x}\bar{x}}^{(0)}, \quad (12c)$$

$$Z = \frac{\cos^2 \bar{x}}{L^2} (Z_{\bar{x}\bar{x}} - Z_{\bar{t}\bar{t}}) + Z^{(0)}, \quad (12d)$$

where the inhomogeneous source terms $Z_{ab}^{(0)}$ and $Z^{(0)}$ can be computed from lower order perturbation results. The vector-type gauge-invariant variable can be obtained from the vector-type generating function $\phi^{(v)} = r\Phi^{(v)}$ as

$$Z_{\bar{t}} = \partial_{\bar{x}} \phi^{(v)} + Z_{\bar{t}}^{(0)}, \quad Z_{\bar{x}} = \partial_{\bar{t}} \phi^{(v)}, \quad (13)$$

where $Z_{\bar{t}}^{(0)}$ is an other inhomogeneous source term. Finally, the metric perturbation variables in each class can be recovered with Equation (9).

At first order in the ε expansion no source terms appear from lower orders, and the scalar equation can be solved explicitly. Regular and asymptotically AdS scalar-type perturbations exist only for frequencies $\bar{\omega}_s = l + 1 + 2n$, with $n \geq 0$ integer. The corresponding generating function is

$$\Phi_1^{(s)} = \frac{\alpha}{L} \sin^{l+1} \bar{x} \cos(\bar{\omega}_s \bar{t} - \delta) \frac{n!}{(l + \frac{3}{2})_n} P_n^{(l+\frac{1}{2}, -\frac{1}{2})}(\cos(2\bar{x})), \quad (14)$$

where α is a constant figuring the amplitude, δ is a constant phase, P are the Jacobi polynomials, and the Pochhammer's Symbol is $(c)_n = \Gamma(c+n)/\Gamma(c)$. Vector-type perturbations exist for frequencies $\bar{\omega}_v = l + 2 + 2n$, having the form

$$\Phi_1^{(v)} = \frac{\alpha}{L} \cos \bar{x} \sin^{l+1} \bar{x} \cos(\bar{\omega}_v \bar{t} - \delta) \frac{n!}{(l + \frac{3}{2})_n} P_n^{(l+\frac{1}{2}, \frac{1}{2})}(\cos(2\bar{x})). \quad (15)$$

Hereafter, the integer n will denote the radial excitation number.

As a valid first order solution, we can choose any linear combination of the metric perturbations generated by equations (14) and (15), with arbitrary amplitudes and phases, for a number of different (l, m) . Proceeding to second order in ε , there will be $\Phi^{(s,v)(0)}$ source terms appearing in Equation (10) for certain scalar and vector (l, m) cases. At ε^2 order these equations are generally solvable. However, at third order, certain $\Phi^{(s,v)(0)}$ will contain terms that have time dependence with resonant frequencies $\bar{\omega}_{s,v}$. In these resonant cases, the master Equation (10) can have regular asymptotically AdS time-periodic solutions only if certain consistency conditions hold (they generally require the vanishing of an integral between $\bar{x} = 0$ and $\bar{x} = \pi/2$ involving the source term).

These make severe restrictions on the allowed amplitudes and phases of the linear modes that we include at first order in ε . Furthermore, in these resonant cases the solution for $\Phi^{(s,v)}$ is not unique, one can always add a constant times the homogeneous solution. This implies that at ε^3 order new constants appear in the expansion procedure, and these constants will be restricted later by the consistency conditions at order ε^5 .

It is natural to start with as few components as possible at the linear level. On the other hand, it is important to see what kind of combinations of same-frequency linear modes can survive to higher order in the formalism. For example, one can try to find the most general monochromatic scalar-type solution with $l = 2$ and $n = 0$ that has a mirror symmetry at the $\theta = \pi/2$ plane. At the linear level, any combination of the $m = 2, -2, 0$ modes with the independent $\delta = 0$ and $\pi/2$ phases is allowed (i.e. six independent amplitudes). Solving the consistency conditions at ε^3 order, it turns out that all solutions in this class with a nonzero angular momentum J must be helically symmetric.

In the present paper we focus on helically symmetric geons. In particular, we study in more details the one-parameter family of helically symmetric geons arising from the $l = 2, m = \pm 2, n = 0$ linear scalar modes, which was already considered in [56] and [60]. In order to build helically symmetric perturbative geons, we combine the metric perturbations corresponding to $(m = 2, \delta = 0)$ and $(m = -2, \delta = \pi/2)$ with equal amplitude, such that the nonzero components of the metric perturbation are

$$h_{\bar{t}\bar{t}} = h_{\bar{x}\bar{x}} = -9L^2 \frac{\sin^2 \bar{x} \cos(2\bar{x})}{2 \cos \bar{x}} \sin^2 \theta \cos(3\bar{t} - 2\phi) , \quad (16)$$

$$h_{\bar{t}\bar{x}} = 9L^2 \sin^3 \bar{x} \sin^2 \theta \sin(3\bar{t} - 2\phi) , \quad (17)$$

$$h_{\theta\theta} = \frac{h_{\phi\phi}}{\sin^2 \theta} = -9L^2 \frac{\sin^4 \bar{x}}{2 \cos \bar{x}} \sin^2 \theta \cos(3\bar{t} - 2\phi) . \quad (18)$$

A simple change of coordinates $\phi \leftarrow \phi - \omega\bar{t}/m$ brings the metric in a manifestly time independent form whose Killing vector is

$$\partial_{t'} \equiv \partial_{\bar{t}} + \frac{\omega}{m} \partial_{\varphi} . \quad (19)$$

We were able to unambiguously construct the ε expansion of the metric for this geon up to fourth order. In order to achieve this we had to solve the consistency conditions at fifth order in ε , which is necessary for getting the concrete values of the integration constants that appear at third order in the expansion. For rotating geons a natural way to fix the re-parametrization freedom in the ε parameter is to cancel all higher order coefficients in the expansion of the angular momentum J . Choosing then the coefficient α in Equation (14) appropriately, we set $J = 27\pi L^2 \varepsilon^2 / 128$, which agrees with the choice made in [56]. The obtained expansions for the frequency and the mass (see Section 5 below for definition) of the configuration can be written as

$$\omega L = 3 \left(1 + \omega_1 \frac{J}{L^2} + \omega_2 \frac{J^2}{L^4} + \dots \right) , \quad (20a)$$

$$\omega L = 3 \left(1 + \omega_1 \frac{2M}{3L} + \frac{2}{3} (2\omega_2 - \omega_1^2) \frac{M^2}{L^2} + \dots \right) , \quad (20b)$$

$$\frac{M}{L} = \frac{3}{2} \left(\frac{J}{L^2} + \frac{\omega_1 J^2}{2 L^4} + \frac{\omega_2 J^3}{3 L^6} + \dots \right), \quad (20c)$$

where

$$\omega_1 = -\frac{4901}{3780\pi} \approx -0.412708, \quad (21a)$$

$$\omega_2 = \frac{7823862709549425\pi^2 - 76880912765261056}{73229764608000\pi^2} \approx 0.466991. \quad (21b)$$

In order to get the J^3 term in the mass we had to calculate the $l = 0$ and $l = 1$ components at sixth order in ε .

In the remaining of the paper, first order geons are used as initial guess configurations. Successive perturbative orders allow us to quantify the proximity between the analytical and numerical approaches.

3. Gauge-fixing

3.1. Perturbative geon in the Andersson-Moncrief gauge

We start with the 3+1 formalism [66], where the metric reads

$$g_{\alpha\beta} dx^\alpha dx^\beta = -N^2 dt^2 + \gamma_{ij} (dx^i + \beta^i dt)(dx^j + \beta^j dt), \quad (22)$$

where latin indices denote spatial directions on $t = cst$ hypersurfaces Σ_t , N is the so-called lapse function, β^i the shift vector and γ_{ij} the spatial 3-metric. The normal vector to Σ_t is $u_\alpha = (-N, 0, 0, 0)$. We also introduce K_{ij} the extrinsic curvature of Σ_t

$$K_{ij} = -\frac{1}{2N} \mathcal{L}_m \gamma_{ij}, \quad (23)$$

where \mathcal{L}_m is the Lie derivative in the direction $m^\alpha \equiv Nu^\alpha = \partial_t^\alpha - \beta^\alpha$.

In order to solve the system, one needs to specify appropriate gauge conditions. The foliation is defined by the maximal slicing condition and the spatial coordinates are chosen to be harmonic. We dubbed this choice the Andersson-Moncrief gauge in reference to [65]. The Andersson-Moncrief gauge corresponds to imposing the following conditions:

$$K \equiv \gamma^{ij} K_{ij} = 0, \quad (24a)$$

$$V^i \equiv \gamma^{kl} (\Gamma_{kl}^i - \bar{\Gamma}_{kl}^i) = -\sqrt{\frac{\bar{\gamma}}{\gamma}} \bar{D}_k \left(\sqrt{\frac{\gamma}{\bar{\gamma}}} \gamma^{ik} \right) = 0, \quad (24b)$$

where Γ_{kl}^i is the Christoffel symbol of γ_{ij} , and $\bar{\Gamma}_{kl}^i$ and \bar{D} the Christoffel symbols and connection of the AdS background 3-metric $\bar{\gamma}_{ij}$. A well-known gauge used in the literature is the harmonic gauge [71–74], which is basically a 4D version of Equation (24b). In Appendix A, we clarify the connection between the two gauges.

To put the first order perturbative geon in the Andersson-Moncrief gauge, we proceed in two steps. First, we infinitesimally change the time coordinate $t \leftarrow t + \alpha(x^i)$ while keeping unchanged the spatial ones. The transformation rules for $g_{\alpha\beta}$ at first order in α give

$$N \leftarrow N(1 + \beta^i \partial_i \alpha), \quad \beta^i \leftarrow \beta^i + (N^2 \gamma^{ij} + \beta^i \beta^j) \partial_j \alpha, \quad \gamma_{ij} \leftarrow \gamma_{ij} - \beta_i \partial_j \alpha - \beta_j \partial_i \alpha.$$

Equation (24a) can be enforced by solving :

$$2N^2\partial^i\partial_i\alpha + 2\partial_i(N^2\gamma^{ij})\partial_j\alpha + N^2\partial^k\alpha\gamma^{ij}\partial_k\gamma_{ij} - 2NK(1 + \beta^j\partial_j\alpha) = 0, \quad (25)$$

where all the geometrical quantities refers to the original coordinates.

Second, we perform an infinitesimal transformation of the spatial coordinates $x^i \leftarrow x^i + \xi^i(x^j)$ while keeping the coordinate t unchanged. This doesn't change the foliation, so K is left untouched. At first order, the transformation rules for $g_{\alpha\beta}$ give

$$\begin{aligned} N &\leftarrow N - \mathcal{L}_\xi N, & \beta^i &\leftarrow \beta^i - \mathcal{L}_\xi\beta^i, & \gamma_{ij} &\leftarrow \gamma_{ij} - \mathcal{L}_\xi\gamma_{ij}, \\ \Gamma_{kl}^i &\leftarrow \Gamma_{kl}^i - \mathcal{L}_\xi\Gamma_{kl}^i - \partial_k\partial_l\xi^i, \end{aligned}$$

where \mathcal{L}_ξ stands for the Lie derivative along ξ . Equation (24b) is now equivalent to :

$$-\partial^j\partial_j\xi^i - \gamma^{kl}\mathcal{L}_\xi\Gamma_{kl}^i - (\Gamma_{kl}^i - \bar{\Gamma}_{kl}^i)\mathcal{L}_\xi\gamma^{kl} + V^i = 0, \quad (26)$$

where, again, the geometrical quantities are the ones in the original coordinates.

Equations (25) and (26) can be solved numerically with the Kadath library. This allows us to compute first order geons in the Andersson-Moncrief gauge.

3.2. Solving Einstein equations in the Andersson-Moncrief gauge

We recall the 3+1 equations with cosmological constant

$$R + K^2 - K_{ij}K^{ij} - 2\Lambda = 0, \quad (27a)$$

$$D_jK_i^j - D_iK = 0, \quad (27b)$$

$$-\mathcal{L}_mK_{ij} - D_iD_jN + N(R_{ij} + KK_{ij} - 2K_{ik}K_j^k - \Lambda\gamma_{ij}) = 0, \quad (27c)$$

where R_{ij} is the Ricci tensor of the 3-metric γ_{ij} .

First, in [65], it was shown that

$$R_{ij} = -\frac{\gamma^{kl}}{2}\bar{D}_k\bar{D}_l\gamma_{ij} + D_{(i}V_{j)} + \text{terms in } \partial\gamma\partial\gamma, \quad (28)$$

i.e. that, as far as second derivatives are concerned, the Ricci tensor can be decomposed into a well-posed Laplacian-like operator plus a term $D_{(i}V_{j)}$. Let us mention that this is similar to the properties of the Dirac gauge when a conformal decomposition of the spatial metric is performed [75]. We then write a 3+1 Einstein-Andersson-Moncrief system by replacing in (27a)-(27c) all occurrences of K by zero, as is customary for maximal slicing, and all occurrences of R_{ij} by $R_{ij} - D_{(i}V_{j)}$, leading to

$$R - D_iV^i - K_{ij}K^{ij} - 2\Lambda = 0, \quad (29a)$$

$$D_jK_i^j = 0, \quad (29b)$$

$$-\mathcal{L}_mK_{ij} - D_iD_jN + N(R_{ij} - D_{(i}V_{j)} - 2K_{ik}K_j^k - \Lambda\gamma_{ij}) = 0. \quad (29c)$$

Unlike the original system (equations (27a)-(27c)), this one is invertible. However one needs to check, a posteriori, that the obtained solution satisfy the gauge conditions $K = 0$ and $V^i = 0$. In [74] the same kind of technique is used to enforce four-dimensional harmonic gauge, leading to the so-called De Turck method (see Section Appendix A for a comparison of the two gauges).

4. Regularization

We chose to work in the so-called conformal coordinates, in which the AdS length element takes the form

$$\bar{d}s^2 = \bar{g}_{\alpha\beta} dx^\alpha dx^\beta = - \left(\frac{1 + \rho^2}{1 - \rho^2} \right)^2 dt^2 + \frac{4}{(1 - \rho^2)^2} (dx^2 + dy^2 + dz^2), \quad \rho = r/L, \quad (30)$$

where $r = \sqrt{x^2 + y^2 + z^2} \in [0, L]$.

Defining the conformal factor

$$\Omega = \frac{1 - \rho^2}{1 + \rho^2}, \quad (31)$$

it is clear that the AdS metric diverges at the boundary $r = L$ like $O(\Omega^{-2})$. We then introduce the conformal background metric

$$\hat{d}s^2 \equiv \Omega^2 \bar{d}s^2 = \hat{g}_{\alpha\beta} dx^\alpha dx^\beta = -dt^2 + \frac{4}{(1 + \rho^2)^2} (dx^2 + dy^2 + dz^2), \quad (32)$$

which is regular and flat at $r = L$. This makes the conformal metric much better suited for numerical computations than the physical diverging one. Hereafter, we denote by a hat all geometrical quantities that we regularize using some power of Ω , such that all hatted quantities are regular. In Table 1 the behavior of various geometric quantities and their conformal regularization are summarized.

Quantity	behavior at $r = L$	Regularization	behavior at $r = L$
$g_{\alpha\beta}$	$O(\Omega^{-2})$	$\hat{g}_{\alpha\beta} \equiv \Omega^2 g_{\alpha\beta}$	$O(1)$
N	$O(\Omega^{-1})$	$\hat{N} \equiv \Omega N$	$O(1)$
β^i	$O(1)$	$\hat{\beta}^i \equiv \beta^i$	$O(1)$
γ_{ij}	$O(\Omega^{-2})$	$\hat{\gamma}_{ij} \equiv \Omega^2 \gamma_{ij}$	$O(1)$
γ^{ij}	$O(\Omega^2)$	$\hat{\gamma}^{ij} \equiv \gamma^{ij} / \Omega^2$	$O(1)$
Γ_{ij}^k	$O(\Omega^{-1})$	$\hat{\Gamma}_{ij}^k \equiv \Omega \Gamma_{ij}^k$	$O(1)$
K_{ij}	$O(\Omega^{-2})$	$\hat{K}_{ij} \equiv \Omega^2 K_{ij}$	$O(1)$
K_i^j	$O(1)$	$\hat{K}_i^j \equiv K_i^j$	$O(1)$
K	$O(1)$	$\hat{K} \equiv K$	$O(1)$
K^{ij}	$O(\Omega^2)$	$\hat{K}^{ij} \equiv K^{ij} / \Omega^2$	$O(1)$
R_{ij}	$O(\Omega^{-2})$	$\hat{R}_{ij} \equiv \Omega^2 R_{ij}$	$O(1)$
R	$O(1)$	$\hat{R} \equiv R$	$O(1)$
V^i	$O(\Omega)$	$\hat{V}^i \equiv V^i / \Omega$	$O(1)$
V_i	$O(\Omega^{-1})$	$\hat{V}_i \equiv \Omega V_i$	$O(1)$

Table 1. Behavior of geometrical quantities near the AdS boundary expressed in powers of the conformal factor Ω .

It is then straightforward to show that the left-hand sides of equations (29a)-(29c) behave respectively like $O(1)$, $O(\Omega^{-1})$ and $O(\Omega^{-3})$ at the AdS boundary. We then

denote $\Omega_i = \partial_i \Omega$ and introduce a regularized $O(1)$ version of the system:

$$\hat{R} - \partial_i(\Omega \hat{V}^i) - \hat{\Gamma}_{ij}^i \hat{V}^j - \hat{K}_{ij} \hat{K}^{ij} - 2\Lambda = 0, \quad (33a)$$

$$\Omega \partial_j \hat{K}_i^j + \hat{\Gamma}_{jk}^j \hat{K}_i^k - \hat{\Gamma}_{ij}^k \hat{K}_k^j = 0, \quad (33b)$$

$$-\Omega \mathcal{L}_m \hat{K}_{ij} - 2\hat{K}_{ij} \hat{\beta}^k \Omega_k - \delta \hat{N}_{ij} \quad (33c)$$

$$+ \hat{N}(\hat{R}_{ij} - \Omega \partial_{(i} \hat{V}_{j)}) + \hat{V}_{(i} \Omega_{j)} + \hat{\Gamma}_{ij}^k \hat{V}_k - 2\hat{K}_{ik} \hat{K}_j^k - \Lambda \hat{\gamma}_{ij}) = 0,$$

where the following regularizations hold

$$\delta \hat{N}_{ij} \equiv \Omega^3 D_i D_j \left(\frac{\hat{N}}{\Omega} \right) \quad (34a)$$

$$= \Omega^2 \partial_i \partial_j \hat{N} - \Omega(\Omega_i \partial_j \hat{N} + \Omega_j \partial_i \hat{N} + \hat{N} \partial_i \partial_j \Omega + \hat{\Gamma}_{ij}^k \partial_k \hat{N}) + 2\hat{N} \Omega_i \Omega_j + \hat{N} \hat{\Gamma}_{ij}^k \Omega_k,$$

$$\hat{K}_{ij} \equiv \Omega^2 K_{ij} = -\frac{1}{2\hat{N}}(\Omega \mathcal{L}_m \hat{\gamma}_{ij} + 2\hat{\gamma}_{ij} \hat{\beta}^k \Omega_k), \quad (34b)$$

$$\hat{\Gamma}_{ij}^k \equiv \Omega \Gamma_{ij}^k = \frac{\Omega}{2} \hat{\gamma}^{kl} (\partial_i \hat{\gamma}_{jl} + \partial_j \hat{\gamma}_{il} - \partial_l \hat{\gamma}_{ij}) - \hat{\gamma}^{kl} (\hat{\gamma}_{il} \Omega_j + \hat{\gamma}_{jl} \Omega_i - \hat{\gamma}_{ij} \Omega_l), \quad (34c)$$

$$\hat{R}_{ij} \equiv \Omega^2 R_{ij} = \Omega(\partial_k \hat{\Gamma}_{ij}^k - \partial_i \hat{\Gamma}_{jk}^k) - (\hat{\Gamma}_{ij}^k \Omega_k - \hat{\Gamma}_{jk}^k \Omega_i) + \hat{\Gamma}_{ij}^k \hat{\Gamma}_{kl}^l - \hat{\Gamma}_{jk}^l \hat{\Gamma}_{il}^k. \quad (34d)$$

System (33a)-(33c) is then a regularized 3+1 Einstein-Andersson-Moncrief system in asymptotically AdS spacetimes. This is the system of relevance for our numerical computations.

Incidentally, equations (25) and (26) have to be regularized too for numerical needs (see Section Appendix B).

5. Asymptotically AdS spacetimes

To give a precise definition of AdS asymptotics, we refer§ to [68, 69]. A necessary conditions for a spacetime to be asymptotically AdS is to have a Weyl tensor that vanishes at the boundary. As the Weyl tensor is a conformal invariant, it can be computed either with the physical metric $g_{\alpha\beta}$ or with its conformal counterpart $\hat{g}_{\alpha\beta}$:

$$C_{\beta\mu\nu}^\alpha = \hat{C}_{\beta\mu\nu}^\alpha \hat{=} 0, \quad (35)$$

where $C_{\beta\mu\nu}^\alpha$ is the Weyl tensor of $g_{\alpha\beta}$, $\hat{C}_{\beta\mu\nu}^\alpha$ that of $\hat{g}_{\alpha\beta}$ and $\hat{=}$ means equality restricted to the AdS boundary $r = L$. However, in four dimensions, the vanishing of the Weyl tensor is not a strong enough condition to ensure the AdS asymptotics. A sufficient condition is then to require its leading order magnetic part to vanish, namely

$$\hat{B}_{\alpha\beta} \equiv \frac{1}{\Omega} * \hat{C}_{\alpha\mu\beta\nu} \hat{\nabla}^\mu \Omega \hat{\nabla}^\nu \Omega \hat{=} 0, \quad (36)$$

where $\hat{\nabla}$ is the connection of $\hat{g}_{\alpha\beta}$ and $*$ denotes Hodge duality.

§ Beware that in our notations, $g_{\alpha\beta}$ denotes the physical metric and $\hat{g}_{\alpha\beta}$ denotes the conformal one while in [68, 69] the opposite convention is chosen.

This definition comes with conserved charge definitions. Given an asymptotically conformal Killing vector $\hat{\xi}^\alpha$, an associated conserved charge is obtained with^{||}

$$Q_\xi^{AMD}[\Sigma_t] \equiv -\frac{L^3}{8\pi G} \oint_{\partial\Sigma_t} \frac{1}{\Omega} \hat{\mathcal{C}}_{\alpha\mu\beta\nu} \hat{\nabla}^\mu \Omega \hat{\nabla}^\nu \Omega \hat{\xi}^\alpha \hat{u}^\beta \sqrt{\hat{\sigma}} d^2y, \quad (37)$$

where $\hat{\sigma}_{\alpha\beta}$ is the metric induced by $\hat{g}_{\alpha\beta}$ on $\partial\Sigma_t$ (i.e. the 2-sphere $r = L$) and \hat{u}^α is the unit normal vector to Σ_t with respect to $\hat{g}_{\alpha\beta}$. Choosing ξ^α to be either ∂_t^α or ∂_φ^α gives then a numerical measure of the mass M^{AMD} and of the angular momentum J^{AMD} of geons.

There is an other definition of conserved charge detailed in [70]. It is related to the stress tensor of the dual CFT. Consider the hypersurfaces $r = \text{cst}$ and denote by $q_{\alpha\beta}$ the metric induced by $g_{\alpha\beta}$ and by $\Theta_{\alpha\beta}$ the associated extrinsic curvature. A quasilocal stress tensor can then be defined as

$$T_{\alpha\beta}^{CFT} = \frac{1}{8\pi G} \left(\Theta_{\alpha\beta} - \Theta q_{\alpha\beta} - \frac{2}{L} q_{\alpha\beta} + L \mathcal{G}_{\alpha\beta} \right), \quad (38)$$

where $\mathcal{G}_{\alpha\beta}$ is the Einstein tensor of $q_{\alpha\beta}$. At first sight, one may think that $T_{\alpha\beta}^{CFT}$ behaves as $O(\Omega^{-2})$ near the AdS boundary, but it is actually a $O(\Omega^2)$ for pure AdS, and a $O(\Omega)$ for asymptotically AdS solutions (the physical stress tensor of the CFT is actually given by $T_{\alpha\beta}^{CFT}/\Omega$ at $r = L$). In Section Appendix C, we explain how it can be regularized and computed numerically.

Given an asymptotically Killing vector ξ^α , an associated conserved charge is[¶]

$$Q_\xi^{BK}[\Sigma_t] = \oint_{\partial\Sigma_t} T_{\mu\nu}^{CFT} u^\mu \xi^\nu \sqrt{\sigma} d^2y, \quad (39)$$

where $\sigma_{\alpha\beta}$ is the metric induced by $g_{\alpha\beta}$ on $\partial\Sigma_t$ and u^α is the unit normal vector to Σ_t with respect to $g_{\alpha\beta}$. Since $\sqrt{\sigma} = O(\Omega^{-2})$ and $u^\mu = O(\Omega)$ near the AdS boundary, it is clear that a charge can exist if and only if $T_{\alpha\beta}^{CFT} = O(\Omega)$. Choosing ξ^α equal to ∂_t^α or ∂_φ^α provides us with a second, independent measure of mass M^{BK} and angular momentum J^{BK} of geons.

Furthermore, it was demonstrated in [69] (see also [76]) that these two definitions of charge are equivalent in any four-dimensional asymptotically AdS spacetime. In Section Appendix D, we test this assumption and our numerics with the Kerr-AdS metric.

6. Numerical setup

6.1. Numerical algorithm

In the present work, differential equations are solved using the open source KADATH library [67], which provides a C++ interface for solving relativistic systems of equations with multi-domain spectral methods. This user-friendly library has been successfully

^{||} AMD = Ashtekar-Magnon-Das

[¶] BK = Balasubramanian-Kraus

used in a wide range of context (from binary black holes [77] to boson stars [78] to give a few) certifying its robustness. The library manages non-linear systems with a Newton-Raphson scheme.

In order to construct non-linear numerical geons, we proceed as follows :

- We analytically construct a helically symmetric first order geon with the results of Section 2, and transform the perturbative solution to be expressed in corotating conformal coordinates in which the helical Killing vector is just driven by our time coordinate t'

$$\partial_{t'}^\alpha = \partial_t^\alpha + \frac{\omega}{m} \partial_\varphi^\alpha, \quad (40)$$

such that $\partial_{t'} g_{\alpha\beta} = 0$ and $\mathcal{L}_m = -\mathcal{L}_{\hat{\beta}}$ in (33a)-(33c).

- Choosing a suitably small amplitude, the linearized first order geon is further processed numerically to be expressed in the Andersson-Moncrief Gauge. This is achieved by solving Equation (B.1) and Equation (B.2) with the Kadath library, as explained in Section 3 and Section Appendix B.
- The resulting first order geon in the Andersson-Moncrief gauge is then used as an initial guess for the full 3+1 Einstein-Andersson-Moncrief system of ten equations (33a)-(33c) whose ten unknowns are N, β^i, γ_{ij} . The boundary conditions at the AdS boundary are the following :

$$\hat{N} \cong \hat{N}, \quad \hat{\beta}^i \cong \frac{\omega}{m} \partial_\phi^i, \quad \hat{\gamma}_{ij} \cong \hat{\gamma}_{ij}. \quad (41)$$

The condition on the shift just translates that the frame is corotating with the geon. As ω is expected to change with the geon amplitude, it is treated as an additional unknown of the system, while we provide an additional equation that enforces the marching parameter, or geon wiggleness w , to take some user-defined value. The Newton-Raphson algorithm of the Kadath library is then in charge of finding the solution. The Newton-Raphson iteration is stopped when the error, measured as the highest coefficient of the Einstein equation residuals, reaches about 10^{-8} .

- Once a numerical and non-linear solution is obtained, it is used as an initial guess for the Einstein-Andersson-Moncrief system with a w slightly incremented. The system then converges to the nearby solution of the system with this wiggleness requirement. Iterating the process, we are able to build sequences of geons parametrized by w , which represents the amplitude of the non-linear geon.

6.2. Precision monitoring

In order to monitor the precision of our numerical results, various tests are performed :

- 1- **Spectral convergence** : if the metric components are well described by the spectral expansion, their spectral coefficients should decrease exponentially. With double precision arithmetics and with a second order differential system of equations, the saturation level is expected to be around 10^{-10} .

- 2- **Gauge residual** : K and V^i should be as low as possible (but are expected to saturate at a 10^{-10} level). Their infinity norm should decrease with numerical resolution. An other complementary check in the Einstein-Andersson-Moncrief framework is to observe a similar convergence for the components of $R_{\alpha\beta} - \Lambda g_{\alpha\beta}$ which should be zero for any solution of Einstein equations in vacuum.
- 3- **Asymptotically AdS spacetimes** : we enforce Dirichlet boundary conditions on the system, however this might not be enough to ensure the right asymptotics. According to Section 5, we can check on one hand that $\hat{C}_{\alpha\beta\mu\nu}$, $\hat{B}_{\alpha\beta}$ and $T_{\alpha\beta}^{CFT}$ have boundary values decreasing to zero, and on the other hand that AMD and BK charges converge to each other when increasing numerical resolution.
- 4- **Agreement with perturbative approach** : any numerical sequence of geon should coincide with perturbative results for low enough amplitudes.

7. Results

7.1. Geons with $(l, m, n) = (2, 2, 0)$

Following Section 6, we start building geons with excitation number $(l, m, n) = (2, 2, 0)$, i.e. helical geons with lowest excitations numbers. We are able to reach unprecedentedly high amplitudes, with deviations from third order perturbative expansion as large as 50%. We will use this family of geons as a testbed for our numerics. Defining

$$h_{\alpha\beta} \equiv g_{\alpha\beta} - \bar{g}_{\alpha\beta} \quad \text{and} \quad \hat{h}_{\alpha\beta} \equiv \Omega^2 h_{\alpha\beta}, \quad (42)$$

a relevant marching parameter, or wiggleness, seems to be

$$w \equiv \hat{h}_{xx}(r=0) = h_{xx}(r=0), \quad (43)$$

in the Andersson-Moncrief gauge, as h_{xx} has a bell shape (see Figure 9). The sequence typically starts at $w = 0.1$ and finishes at $w = 10$ (compare to the AdS background $\hat{g}_{xx}(0) = 4$). We use two domains, one nucleus describing $r \in [0, 0.5]L$ and one shell describing $r \in [0.5, 1]L$. We do so in order to compute $\Theta_{\alpha\beta}$ involved in Equation (38), because as it diverges like $O(r^{-1})$ near the origin, we can only compute it in the shell domain. As l and m are even, there is an octant symmetry. Accordingly, quoting a resolution of, say “37x9x9”, means that, in each domain, one uses $N_r = 37$ points in the r coordinate and $N_\theta = N_\varphi = 9$ points per octant in θ and φ coordinates. We checked that the results are insensitive to the positioning of the domain separation, as expected for the global representation of smooth fields in spectral methods.

In Figure 1, we show how the Einstein and gauge residuals of the system of equations vary with amplitude and resolution. As curves happen to be almost insensitive to radial resolution $N_r \in [29, 37]$, we only show the angular resolution dependence. The errors are increasing with the amplitude of the geon, but decrease exponentially by several orders of magnitude with resolution, indicating spectral convergence. Thus our solutions are not only solutions of the Einstein-Andersson-Moncrief system but also of the full Einstein

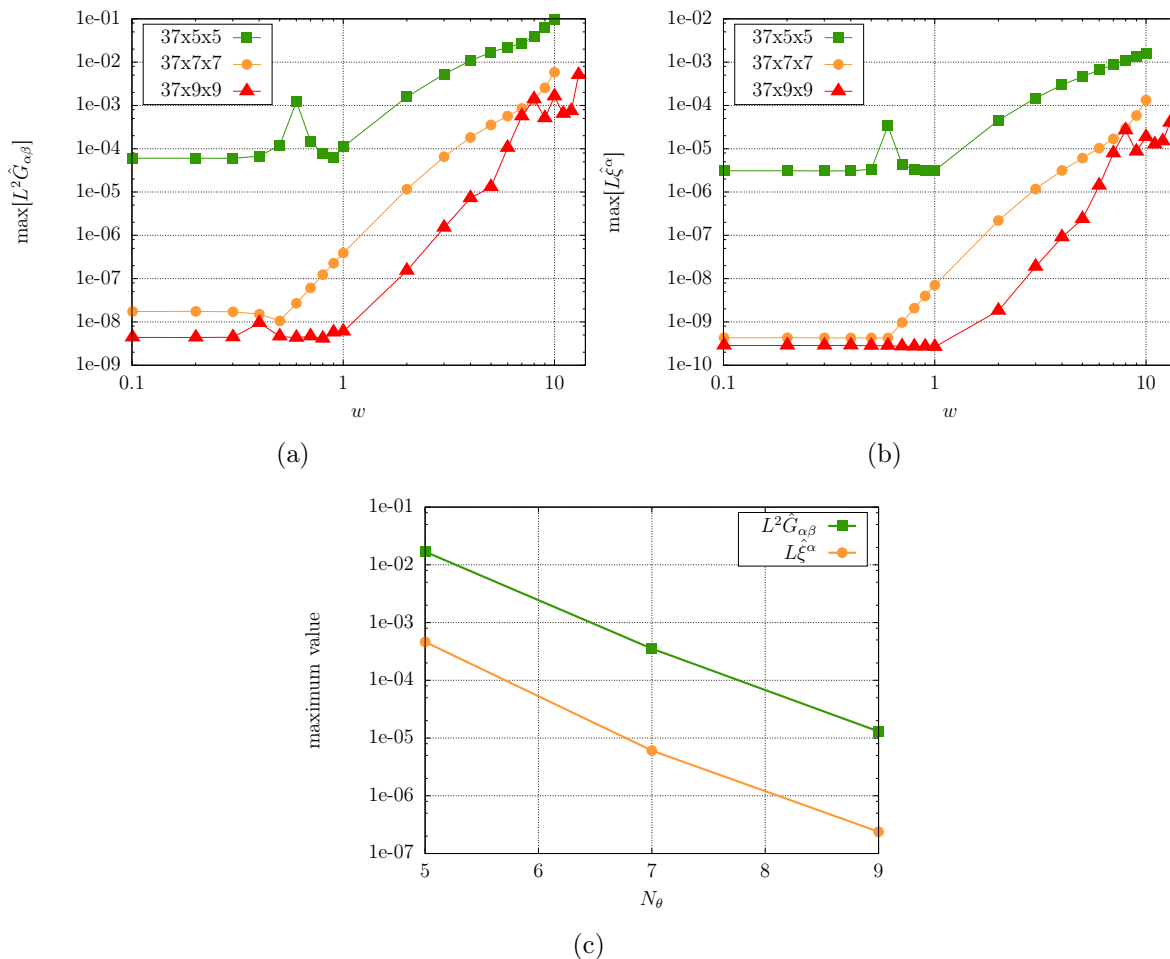


Figure 1. Top left panel : residual of the regularized Einstein equation tensor $\hat{G}_{\alpha\beta} = \hat{R}_{\alpha\beta} - \Lambda \hat{g}_{\alpha\beta}$. Top right panel : residual of the regularized gauge vector $\hat{\xi}^\alpha = (-\hat{K}, \hat{V}^i)$. Bottom panel: spectral convergence of the Einstein and gauge residuals as a function of the angular resolution at fixed wiggleness $w = 5$. Each residual is the maximum value in the whole configuration space, i.e. at collocation points, for the $(l, m, n) = (2, 2, 0)$ geon.

system. At a resolution of 37x9x9, we lower the Einstein residual down to $\sim 10^{-3}$ when the largest metric coefficient is ~ 15 at the origin.

In Figure 2, four AdS asymptotics indicators are evaluated (see Section 5 above). For these, the angular resolution has essentially no effect for $N_{\theta,\varphi} \in [5, 9]$, so we show the radial resolution declination only. The higher the radial resolution, the closer to zero they are, which shows that our solutions are well asymptotically AdS. The bottom right panel shows that our AMD and BK charges agree with each other at a $\sim 0.5\%$ level, which is an extra confirmation of the validity of our solutions. The convergence rate seems to be quite slow, but this is to be expected : these indicators are quite demanding in terms of precision as they involve second order derivatives, divisions in coefficient space and evaluation or integration at the AdS boundary.

Figure 3 shows the coefficients of our solution with largest amplitude $w = 10$ and

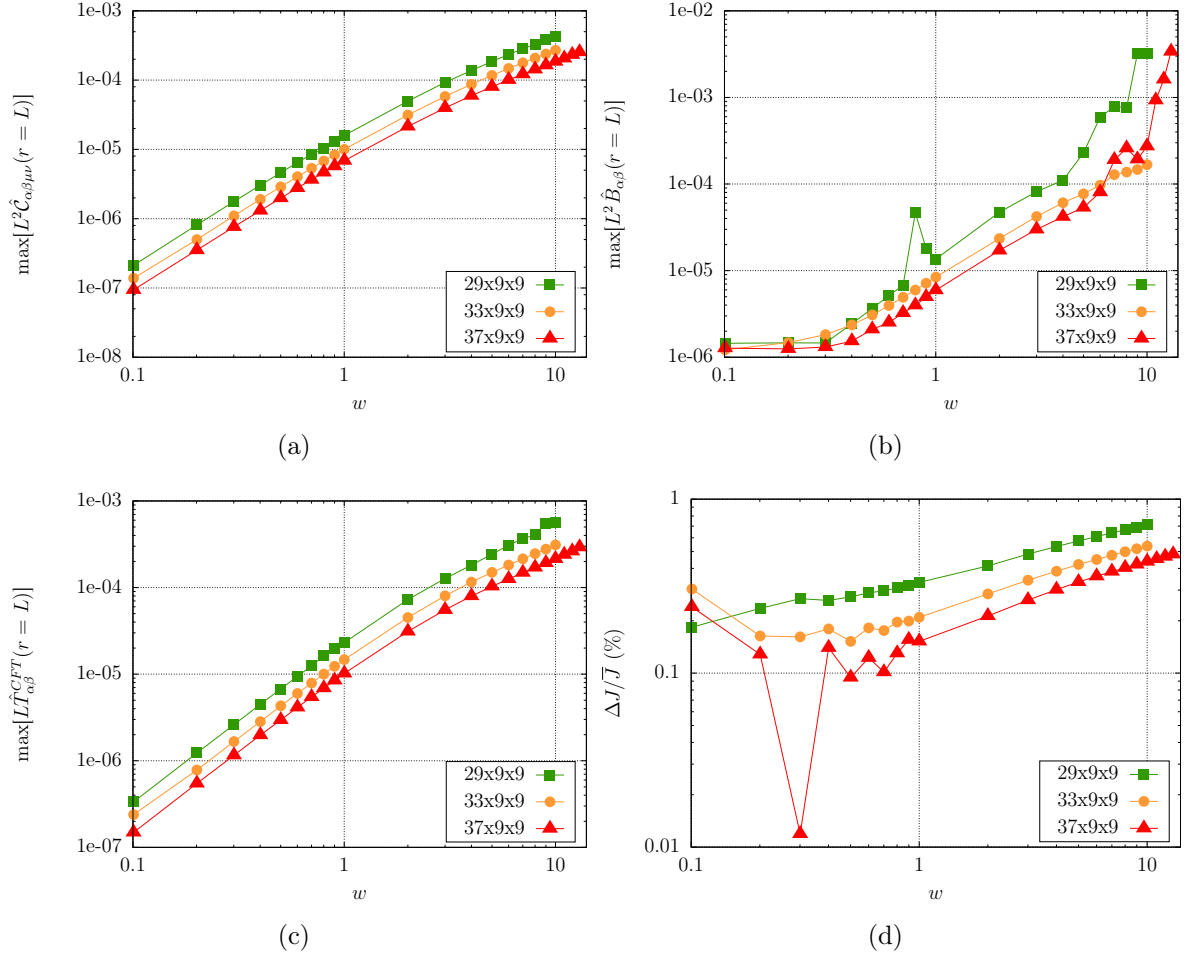


Figure 2. AdS residuals for the $(l, m, n) = (2, 2, 0)$ geon. Upper left panel : residual of the boundary Weyl tensor $\hat{C}_{\alpha\beta\mu\nu}$ of $\hat{g}_{\alpha\beta}$. Upper right panel : residual of its rescaled magnetic part $\hat{B}_{\alpha\beta}$. Bottom left panel : residual of the CFT stress tensor $T_{\alpha\beta}^{CFT}$. All residuals are restricted to the AdS boundary. Bottom right panel : relative difference between AMD and BK angular momenta, with $\Delta J = J^{AMD} - J^{BK}$ and $\bar{J} = (J^{AMD} + J^{BK})/2$.

highest resolution 37x9x9. Spectral convergence is observed both radially and angularly. The saturation threshold is larger for the Weyl tensor $\hat{C}_{\alpha\beta\mu\nu}$ and the CFT stress tensor $T_{\alpha\beta}^{CFT}$ as they involve second order derivatives of the metric and, for the latter, a regularization procedure (Section Appendix C) that both increase numerical errors and hence noise level. If it were not too computationally demanding, we could increase the angular resolution to describe better the coefficient tail, and it would probably decrease the errors on Einstein equation and gauge residuals, as observed in Figure 1. However, angular resolution doesn't seem critical when it comes to computing global charges.

When it comes to computing geon charges, it turns out that the precision on the mass (be it AMD or BK) is less than that on the angular momentum. In particular, even if J is in a very strong agreement with perturbative approach in a low amplitude limit, M is usually overestimated by $\sim 5\text{-}10\%$ depending on the radial resolution. Increasing

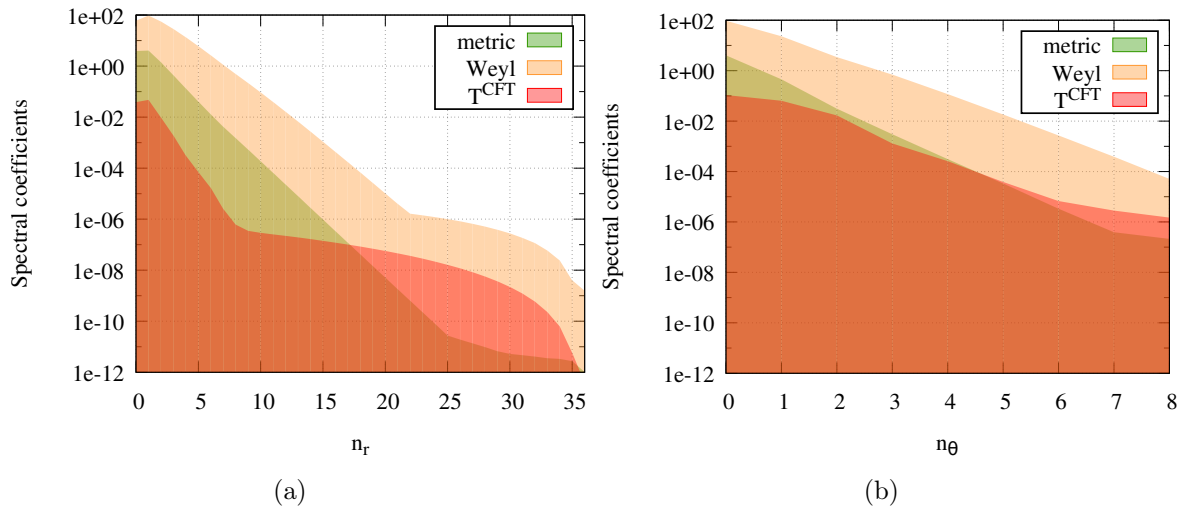


Figure 3. Spectral coefficients of $\hat{g}_{\alpha\beta}$ in green, $\hat{C}_{\alpha\beta\mu\nu}$ in yellow and $T_{\alpha\beta}^{CFT}$ in red for the $(l, m, n) = (2, 2, 0)$ geons at a resolution of $37 \times 9 \times 9$ and amplitude $w = 10$. Our coefficients collection is actually a three-dimensional array indexed by three integers $n_r \in \{0, \dots, N_r\}$, $n_\theta \in \{0, \dots, N_\theta\}$ and $n_\varphi \in \{0, \dots, N_\varphi\}$. Left panel : coefficients versus n_r for arbitrary n_θ and n_φ . Right panel : coefficients versus n_θ for arbitrary n_r and n_φ . For the sake of clarity, only the upper envelope of the coefficients collection is shown.

the number of points improves the match but very slowly. Our guess is that we lose precision on M because of the numerous steps of regularization and spectral operations that all bring their own numerical errors which accumulate. This asymmetry between M and J is unclear, but probably the terms involved in the computation of J are simpler than those involved in the computation of M . We think that, if affordable, quadruple precision could improve this point. So in order to give reliable masses within reasonable computing times, we compute M using the first law of geon dynamics $\delta M - \omega \delta J / m = 0$, which ensures that M is computed with as much precision as ω and J are. This relation is demonstrated in the asymptotically flat case for helically symmetric system [79] with respect to the Arnowitt-Deser-Misner global charges, and a similar results holds for Kerr-AdS [80] with an additional entropy term. Let us also mention that a sketch of a proof is present in [60]. But as far as we know, a rigorous mathematical proof in the general helically symmetric case in asymptotically AdS spacetimes is still missing. Nevertheless the first law is widely accepted and actually confirmed by perturbative results up to sixth order (see Equation (20c)).

In practice, we write

$$M = \int_0^J \frac{\omega(J')}{m} dJ', \quad (44)$$

where the function $\omega(J)$ is obtained by a polynomial fit (reduced $\chi^2 < 10^{-13}$).

Figure 4 displays the three global quantities of importance : the angular velocity ω/m (with $m = 2$), the mass M and angular momentum J . It is clear that successive orders of perturbations are closer and closer to our numerical solutions. In order to

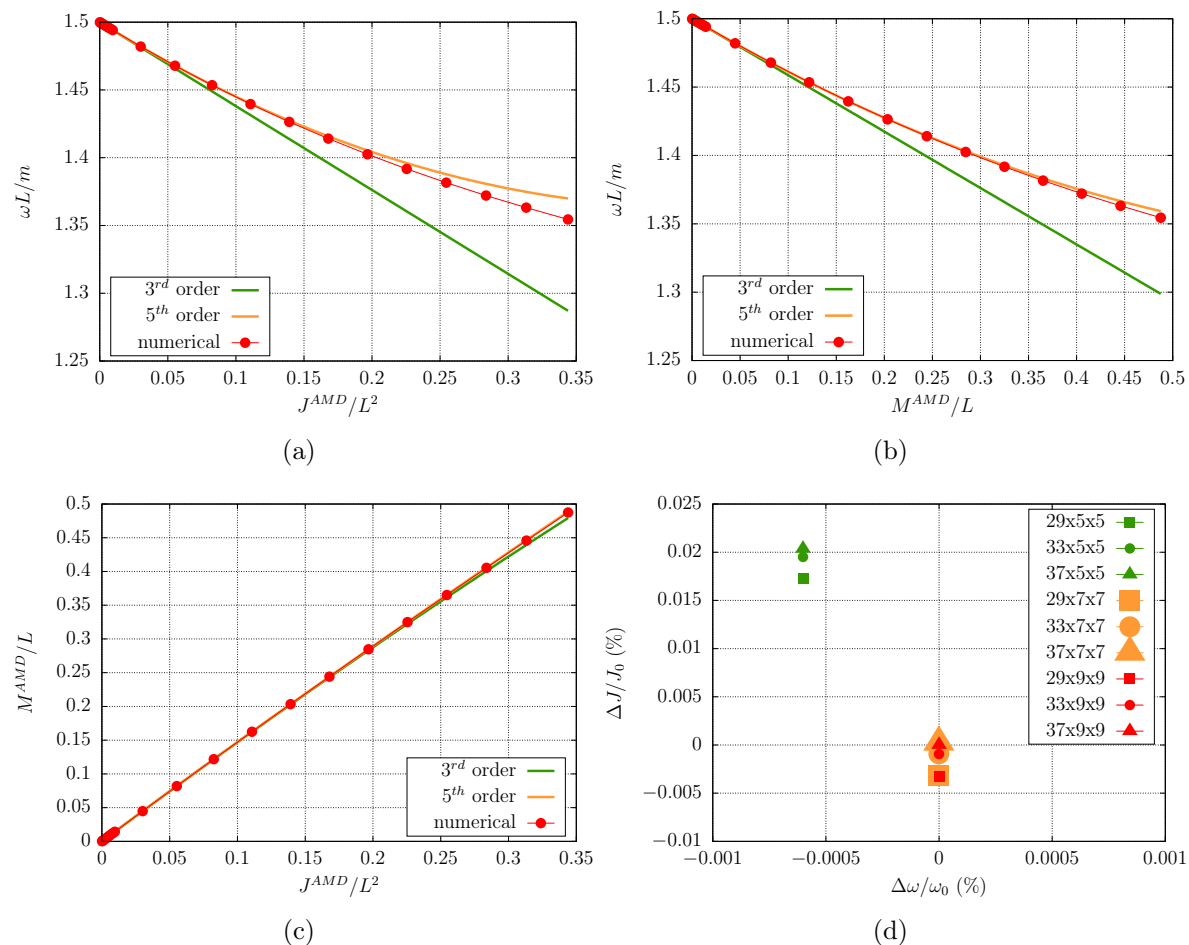


Figure 4. The ω - M - J planes for our numerical sequences $(l, m, n) = (2, 2, 0)$ at resolution $37 \times 9 \times 9$ using AMD definitions. The successive perturbative orders are shown in comparison with our highest resolution results. At the bottom right panel, we have chosen a typical point on the sequence at resolution $37 \times 9 \times 9$ ($w_0 = 5$, $\omega_0 L/m = 1.44$, $J_0 = 0.11$). The plot shows the relative difference $\Delta\omega = \omega - \omega_0$ and $\Delta J = J - J_0$ in percentage for all resolutions, w being fixed at w_0 .

estimate the numerical error bars, we examine one single point of the sequence, say $w = 5$, at all our available resolutions. Taking as reference values the one computed at our highest resolution $37 \times 9 \times 9$, we look at the difference with the lower resolutions results. We naturally expect small differences in the numerical measurements of ω and J depending on the resolution. These differences are pictured on the bottom right panel of figure 4. First, it is clear that the results are converging to the highest resolution results (origin of the plot). Second, this allows us to read off error bars on J and ω , namely $\Delta J \sim 0.02\%$ and $\Delta\omega = 0.0006\%$ between our worst and best resolutions. Restricting the angular resolutions between 7 and 9 angular points (hardly distinguishable on the figure) gives $\Delta J = 0.003\%$ and $\Delta\omega = 0.000001\%$. Furthermore, we observed that these error bars remained approximately constants along the entire sequence. This magnitude of error bars is obviously indistinguishable at naked eye on the three other panels of

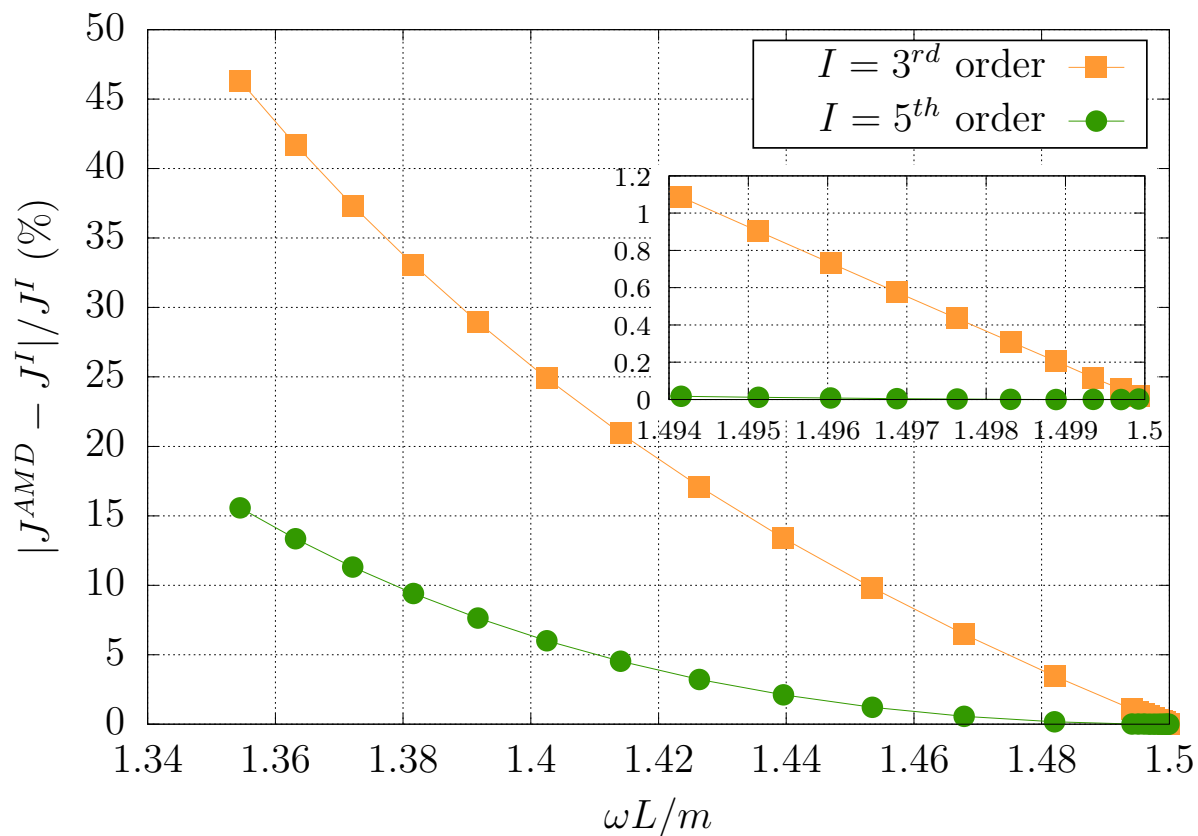


Figure 5. Difference between the numerical J^{AMD} for $(l, m, n) = (2, 2, 0)$ at resolution $37 \times 9 \times 9$ and perturbative approach at I^{th} order, I being 3 (yellow squares) or 5 (green circles). Inset : zoom on the low amplitude limit $\omega L/m \rightarrow 3/2$.

figure 4.

In Figure 5, we show the difference between the numerical results and perturbative predictions. This demonstrates that the non-linear solutions deviates from 3^{rd} order by at most 50% and from 5^{th} order by at most 15%.

If we consider the expansion $\omega L/m = f(J)$

$$\frac{\omega L}{m} = a_0 + a_1 \frac{J}{L^2} + a_2 \frac{J^2}{L^4} + a_3 \frac{J^3}{L^6} + \dots, \quad (45)$$

the a_i coefficients can be computed by a polynomial fit. Table 2 shows the coefficients of the perturbative and numerical results (see Equation (20b)).

	a_0	a_1	a_2	a_3
perturbative	1.5000000	-0.619062	0.70049	-
numerical	1.5000000	-0.619064	0.70031	-0.345
error	$\pm 6.10^{-9}$	$\pm 2.10^{-6}$	$\pm 7.10^{-5}$	$\pm 1.10^{-3}$

Table 2. Coefficients in the polynomial expansion $\omega L/m = f(J)$ for both perturbative and numerical results at resolution $37 \times 9 \times 9$. Error bars are given by the Levenberg-Marquardt fit algorithm.

The numerical and available perturbative values of the coefficients agree very well. For instance the relative difference in a_2 is of order 0.01%.

At this point, let us mention that our results are in disagreement with those of [60], whose authors were the first (and single) to propose a numerical construction of the $(l, m, n) = (2, 2, 0)$ geons. Indeed, looking at their figure (1.b), it is clear that they found a_2 to be negative. According to our results, listed in table 2, we find, however, that $a_2 \sim +0.700$. We are very confident in this result as our perturbative computations carried out to the sixth order agree very well with our precise numerical measurements. We thus provide two independent arguments in favour of the positivity of a_2 , and are unable to find any reason why this coefficient should be negative in [60]. Additional and independent future derivations of these results would provide a very welcome clarification of this point.

7.2. Geons with $(l, m, n) = (4, 4, 0)$

Increasing the angular number of excitations, we can construct geons with $(l, m, n) = (4, 4, 0)$. As a wiggleness parameter, we choose the largest positive coefficient in the spectral expansion of the first order geon, namely :

$$w \equiv \text{coefficient } (n_r = 0, n_\theta = 1, n_\varphi = 1) \text{ of } h_{yy}, \quad (46)$$

Figure 6 shows the Einstein residuals at different resolutions. The exponential decrease in the errors when increasing the number of collocation points demonstrates that our solutions are indeed solutions of Einstein equation. Similar plots hold for the other indicators detailed in the previous subsection.

Global quantities are shown on Figure 7. Our numerical results match the second order perturbative results in the low amplitude limit. We can reach masses of order ~ 0.5 in AdS length units.

Fitting our numerical data, we infer the numerical values of the coefficients in the $\omega L/M = f(J)$ expansion (45). They are presented in Table 3. In order to get the coefficients a_1 and a_2 we had to go to fifth order in the ε expansion, obtaining

$$\omega_1 = -\frac{890231}{4900896\pi} \approx -0.0578199, \quad (47a)$$

$$\omega_2 = \frac{29082107232588401}{1122863180414976} - \frac{777842303655609302903087}{3044556205497398592000\pi^2} \approx 0.0137851. \quad (47b)$$

	a_0	a_1	a_2	a_3
perturbative	1.2500000	-0.05781990	0.0137851	-
numerical	1.2500000	-0.05782040	0.0111142	-0.0011196
error	$\pm 4.10^{-10}$	$\pm 3.10^{-8}$	$\pm 2.10^{-7}$	$\pm 4.10^{-7}$

Table 3. Coefficients in the polynomial expansion $\omega L/m = f(J)$ for both perturbative and numerical results of $(l, m, n) = (4, 4, 0)$ at resolution 37x11x11. Error bars are given by the Levenberg-Marquardt fit algorithm.

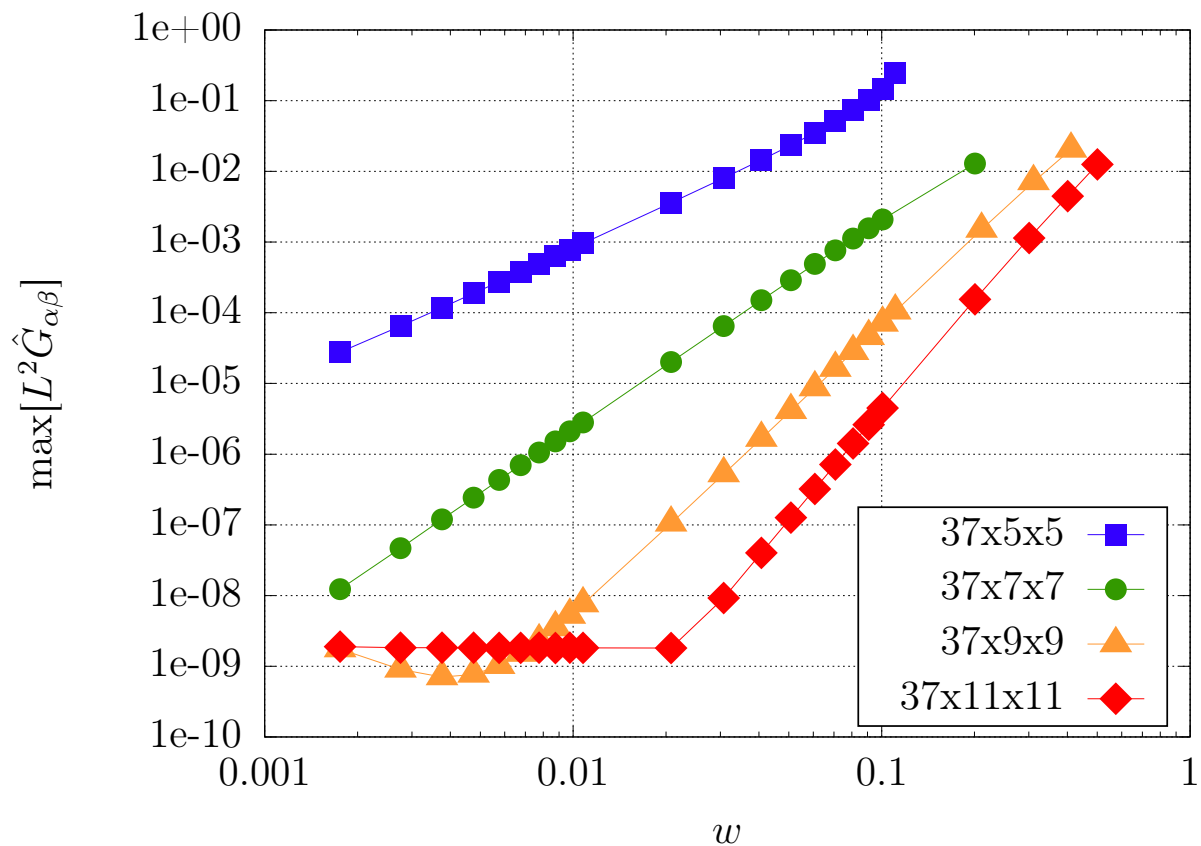


Figure 6. Residual of the regularized Einstein equation tensor $\hat{G}_{\alpha\beta} = \hat{R}_{\alpha\beta} - \Lambda \hat{g}_{\alpha\beta}$ for $(l, m, n) = (4, 4, 0)$.

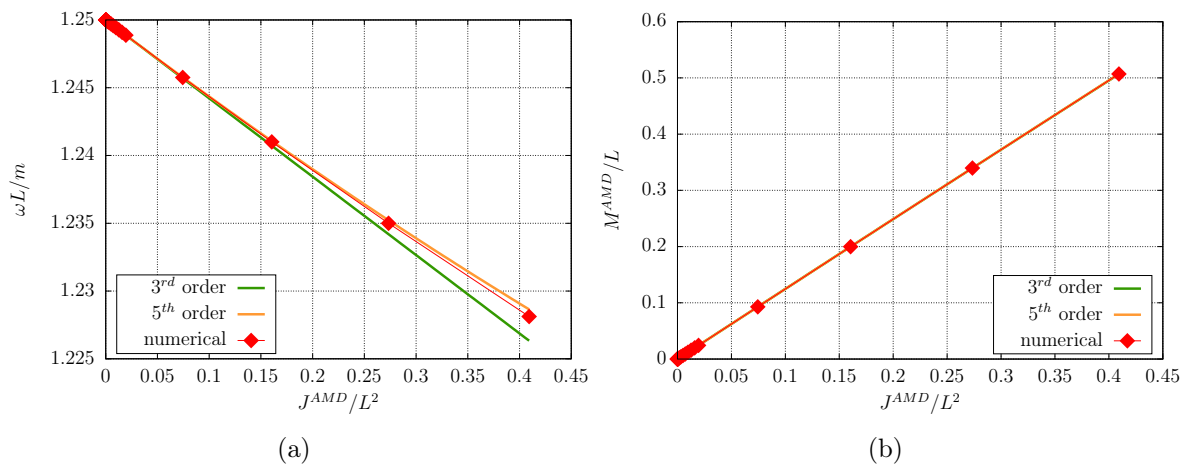


Figure 7. The ω - M - J planes for our numerical sequences $(l, m, n) = (4, 4, 0)$ at resolution $37 \times 11 \times 11$ using AMD definitions. On the right panel, the curves are indistinguishable at naked eye.

Unfortunately, it is hard and time-consuming to push the sequence to higher amplitudes, so we cannot predict the successive coefficients with reasonable precision for the time being.

7.3. Geons with one radial node

The perturbative approach for radially excited geons is more complicated. At first, in [57], the authors claimed that the $(l, m, n) = (2, 2, 1)$ linear mode cannot seed a stable non-linear family of geons, because some secular resonances remain even after the Poincaré-Linstedt regularization. However, recently a paper and a comment came out suggesting that a linear combination of several seeds sharing the same ω could indeed survive at arbitrary order [58, 59].

The angular frequency belonging to the helical extension of the $(2, 2, 1)$ scalar mode is $\bar{\omega}/m = 5/2$, which is the same as the angular frequency of the scalar mode $(4, 2, 0)$ and the vector mode $(3, 2, 0)$. Taking a linear combination of the helically symmetric metric perturbation generated by these three modes, we obtain a three-parameter seed for the perturbation formalism. Evaluating the generating function (14) with $l = 2$, $n = 1$ and $\delta = 0$, calculating the gauge invariant variables using (12a)-(12d) with zero source terms, then using (9) and (6) with $m = 2$ we get the class $(2, 2, 1)$ metric perturbation. Adding the metric perturbation $(2, -2, 1)$ with the same amplitude α , but with phase $\delta = \pi/2$, we get the helically symmetric rotating version of it. We repeat the same procedure for the scalar mode $(4, 2, 0)$, but with amplitude β instead of α . The rotating $(3, 2, 0)$ vector mode, with amplitude γ , is obtained similarly, using (15), (13), (9) and (7). Using this three parameter seed metric for $h_{ab}^{(1)}$, at second order in the ε expansion an unspecified constant ν_2 arises at the $(l, m) = (0, 0)$ mode, according to (4a), which describes the change of the oscillation frequency. The second order perturbation equations always have periodic regular asymptotically AdS solutions, but at third order in ε three consistency conditions arise, at the scalar $(l, m) = (2, 2)$ and $(4, 2)$ modes, and at the $(3, 2)$ vector mode. Each of these three conditions is a long polynomial, they have one term linear in ν_2 , and rest of the terms are cubic and homogeneous in α , β and γ . They can be transformed to a 13-th degree polynomial equation in one variable, which can be solved only numerically, and has 3 real and 10 complex roots. The leading order angular momentum and mass is

$$J = \frac{5(48\alpha^2 + 19845\beta^2 + 245\gamma^2)}{28672L^3}\varepsilon^2, \quad M = \frac{5}{2L}J. \quad (48)$$

The physical frequency of the solution is $\omega = \bar{\omega}/\sqrt{\nu}$, where $\nu = L^2(1 + \nu_2\varepsilon^2)$, according to (5). It follows that the angular frequency to second order in ε is

$$\frac{\omega L}{m} = \frac{5}{2} - \frac{5\nu_2}{4L}\varepsilon^2 = a_0 + a_1\frac{J}{L^2}, \quad (49)$$

where from (48) we get that

$$a_0 = \frac{5}{2}, \quad a_1 = -\frac{3584\nu_2L^4}{48\alpha^2 + 19845\beta^2 + 245\gamma^2}. \quad (50)$$

The numerical values for of ratio of the amplitudes and of the frequency change parameters are given in Table 4. for the three one-parameter families of solutions that satisfy the consistency conditions at ε^3 order.

	$\frac{\beta}{\alpha}$	$\frac{\gamma}{\alpha}$	$\frac{\nu_2 L^4}{\alpha^2}$	a_1
family I.	-0.00286074	0.154618	0.0461014	-3.05866
family II.	0.0367439	-1.67172	0.158401	-0.747498
family III.	1.07086	1.39907	1.17356	-0.180638

Table 4. Numerical values of the parameters for the three one-parameter families of solutions with angular frequency $\bar{\omega}/m = 5/2$.

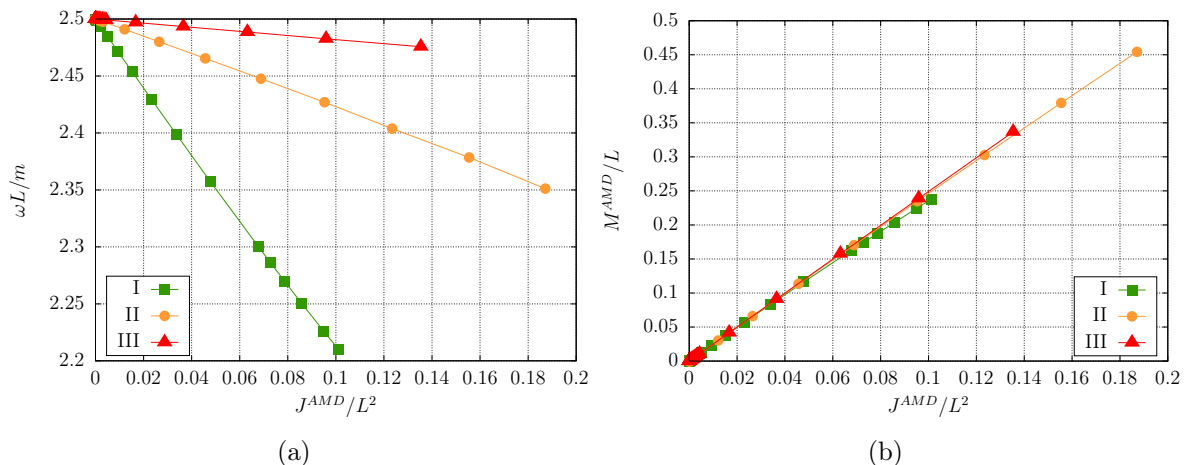


Figure 8. The ω - M - J planes for the three families I,II and III of radially excited geons with one radial node and $m = 2$ using AMD definitions. All curves are computed at a resolution of $37 \times 9 \times 9$.

In order to get radially excited geons, we start with the combination of the three linear modes with amplitudes ratios given in Table 4. Our marching parameters are

$$w \equiv \text{coefficient } (n_r = 1, n_\theta = 0, n_\varphi = 0) \text{ of } \hat{h}_{yy} \text{ for family I,} \quad (51a)$$

$$w \equiv \text{coefficient } (n_r = 0, n_\theta = 1, n_\varphi = 0) \text{ of } \hat{h}_{xx} \text{ for family II,} \quad (51b)$$

$$w \equiv \text{coefficient } (n_r = 0, n_\theta = 1, n_\varphi = 0) \text{ of } \hat{h}_{xz} \text{ for family III.} \quad (51c)$$

We also tried to naively start with a $(l, m, n) = (2, 2, 1)$ first order seed, and observed that the code was converging to the family I branch of solutions, as it is the one with highest contribution from this seed. We built numerically all three families of excited geons.

Global quantities are displayed on Figure 8. The numerical results are in good agreement with second order perturbative ones in the low amplitude limit. We can reach masses of order ~ 0.5 in AdS length unit depending on the family.

Table 5 shows the prediction we can make on the expansion coefficients with our numerical results. We expect that higher amplitudes sequences at higher resolutions could allow us to refine these predictions.

		a_0	a_1	a_2	a_3
family I	perturbative	2.5000000	-3.058658	-	-
	numerical	2.5000000	-3.058670	1.239	8.2
	error	$\pm 2.10^{-9}$	$\pm 7.10^{-6}$	$\pm 2.10^{-3}$	$\pm 3.10^{-1}$
family II	perturbative	2.5000000	-0.747498	-	-
	numerical	2.5000000	-0.747533	-0.1723	-0.39
	error	$\pm 3.10^{-9}$	$\pm 3.10^{-6}$	$\pm 3.10^{-4}$	$\pm 2.10^{-2}$
family III	perturbative	2.5000000	-0.180638	-	-
	numerical	2.5000000	-0.180628	-0.0072	-
	error	$\pm 5.10^{-9}$	$\pm 5.10^{-6}$	$\pm 7.10^{-4}$	-

Table 5. Coefficients in the polynomial expansion $\omega L/m = f(J)$ for both perturbative and numerical results at a resolution of $37 \times 9 \times 9$. Error bars are given by the Levenberg-Marquardt fit algorithm.

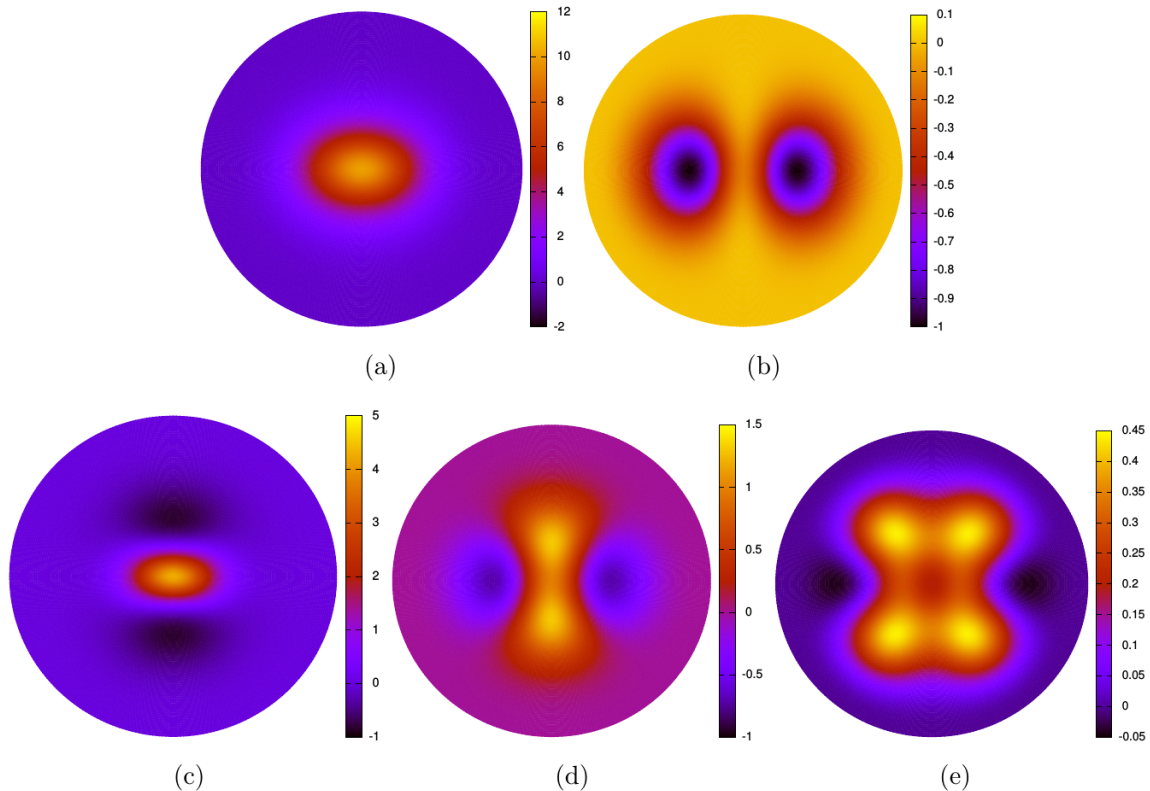


Figure 9. Component \hat{h}_{xx} in the $x = 0$ plane of the conformal metric in the Andersson-Moncrief gauge for all five families of geons studied in this paper, namely the $(l, m, n) = (2, 2, 0)$, $(l, m, n) = (4, 4, 0)$ on the top panel and families I, II and III on the bottom panel. The masses of the solutions pictured are around $\sim 0.2L$, and they were computed at our best numerical resolutions.

8. Conclusion

In this paper, we presented both perturbative and numerical geons in asymptotically AdS spacetimes. We use perturbative approach results at first order to seed an iterative solver of the Einstein-Andersson-Moncrief system, working in a gauge combining maximal slicing and spatial harmonic coordinates. Monitoring precisely numerical errors, we were able to construct geons with different levels of radial and angular excitations at unprecedentedly high amplitudes, reaching masses of order $\sim 1/2$ of the AdS radius. In particular, we gave an independent construction of the fully non-linear $(l, m, n) = (2, 2, 0)$ geons that were constructed solely in [60]. Although we disagree in some ways with [60], the excellent agreement between our analytical and numerical procedures (see Section 7) makes us very confident in the correctness of our results.

We also presented the so-called Andersson-Moncrief gauge and discussed its theoretical motivations as well as its numerical implementation. The link between this gauge and the harmonic gauge enforced with the popular De-Turck method is derived in appendix Appendix A. Last but not least we extended the numerical constructions of fully non-linear geons to the $(l, m, n) = (4, 4, 0)$ case, as well as to the three excited families exhibiting one radial node. The literature about these solutions is quite controversial at the moment, since [57] argues that they cannot exist while [58, 59] supports the idea of their existence. We hope that our numerical construction of these excited geons will put an end to the debate, as we did construct them in our fully non-linear numerical simulations. All five families of geons we built numerically are pictured on Figure 9.

A very interesting continuation of this work would be to use our helical stationary solutions as initial data for an evolution code in AdS. Connection with [65] would be straightforward as we already use 3+1 formalism in the Andersson-Moncrief gauge. This is a daunting task though, but it would give a definitive answer to the problem of purely gravitational islands of stability, and it would be very enlightening to see a high amplitude geon evolving periodically without ever collapsing to a black hole or developing an instability. Our intuition is that geons will bring a whole lot of interesting features in the future investigations on the AdS instability problem beyond spherical symmetry.

Acknowledgments

We would like to thank the referees for their useful and relevant remarks. We are very grateful to Ericourgoulhon, Alexandre Le Tiec and Silvano Bonazzola for enlightening discussions. G. M. is indebted to Fabrice Roy and Marco Mancini for their numerical support. G. F. thanks the kind hospitality of the LUTH research group at Paris Observatory in Meudon during his two-year Marie-Curie fellowship. This research has been supported in part by OTKA Grant No. K 101709 and by the Marie Curie Actions Intra European Fellowship of the European Community's Seventh Framework

Programme under contract number PIEF-GA-2013-621992. This work was granted access to the HPC resources of MesoPSL financed by the Region Ile de France. This work was granted access to the HPC resources of CINES.

Appendix A. Connection between De Turck and Andersson-Moncrief gauges

Instead of Equation (24a) and Equation (24b), the harmonic gauge enforces

$$\xi^\alpha \equiv g^{\mu\nu}(\Gamma_{\mu\nu}^\alpha - \bar{\Gamma}_{\mu\nu}^\alpha) = 0. \quad (\text{A.1})$$

We can 3+1 decompose this vector into $\xi^\alpha = \zeta u^\alpha + \chi^\alpha$ where u^α is the normal vector to Σ_t and χ^α is the spatial projection of ξ^α , i.e. $u_\alpha \chi^\alpha = 0$. We can then compute ζ with⁺

$$\zeta = -u_\alpha \xi^\alpha = N \xi^t = -K - \frac{1}{N^2} \mathcal{L}_m N - \frac{2}{N} \beta^i \partial_i \ln \bar{N}. \quad (\text{A.2})$$

As for the spatial components of χ^α it comes :

$$\begin{aligned} \chi^i &= \xi^i - \zeta u^i = \xi^i + \beta^i \xi^t \\ &= V^i - \frac{1}{N^2} \mathcal{L}_m \beta^i - \partial^i \ln N + \frac{\beta^j \beta^k}{N^2} \bar{\Gamma}_{jk}^i + \frac{1}{N^2} (\bar{N} \bar{\gamma}^{ij} \partial_j \bar{N} + \bar{\beta}^j \bar{D}_j \bar{\beta}^i) \\ &\quad - \frac{2\beta^j}{N^2} ((\beta^j - \bar{\beta}^j) \partial_j \ln \bar{N} + \bar{D}_j \bar{\beta}^i). \end{aligned} \quad (\text{A.3})$$

What is remarkable is that symbolically

$$(\zeta, \chi^i) = (-K, V^i) + \text{terms in } \partial N, \partial \beta^i, \quad (\text{A.4})$$

so the Andersson-Moncrief gauge catches essentially the 3+1 decomposition of the De Turck vector.

On the other hand, the De Turck method doesn't solve the Einstein equation but

$$G_{\alpha\beta} - \nabla_{(\alpha} \xi_{\beta)} = 0. \quad (\text{A.5})$$

We then 3+1 decompose the second term into :

$$\gamma_\mu^\alpha \gamma_\nu^\beta \nabla_{(\alpha} \xi_{\beta)} = -\zeta K_{\mu\nu} + D_{(\mu} \chi_{\nu)}, \quad (\text{A.6})$$

$$\gamma_\mu^\alpha u^\beta \nabla_{(\alpha} \xi_{\beta)} = -\frac{1}{2} D_\mu \zeta + \frac{1}{2} \zeta D_\mu \ln N + K_{\mu\nu} \chi^\nu + \frac{1}{2N} \mathcal{L}_m \chi_\mu, \quad (\text{A.7})$$

$$u^\alpha u^\beta \nabla_{(\alpha} \xi_{\beta)} = -\frac{1}{N} \mathcal{L}_m \zeta - \chi^\mu D_\mu \ln N, \quad (\text{A.8})$$

$$\nabla_\alpha \xi^\alpha = \frac{1}{N} \mathcal{L}_m \zeta - \zeta K + D_\mu \chi^\mu + \chi^\mu D_\mu \ln N, \quad (\text{A.9})$$

which gives the 3+1 Einstein-De Turck system :

$$R + K^2 - K_{ij} K^{ij} - 2\Lambda + \frac{1}{N} \mathcal{L}_m \zeta + \zeta K - D_i \chi^i + \chi^i D_i \ln N = 0, \quad (\text{A.10})$$

$$D_j K_i^j - D_i K - \frac{1}{2} D_i \zeta + \frac{1}{2} \zeta D_i \ln N + K_{ij} \chi^j + \frac{1}{2N} \mathcal{L}_m \chi_i = 0, \quad (\text{A.11})$$

$$\mathcal{L}_m K_{ij} = -D_i D_j N + N(R_{ij} + K K_{ij} - 2K_{ij} K_j^k - \Lambda \gamma_{ij} + \zeta K_{ij} - D_{(i} \chi_{j)}) = 0. \quad (\text{A.12})$$

⁺ Formulas from Appendix B of [81] might help.

Comparing with our Einstein-Andersson-Moncrief system of equations (29a)-(29c), in the light of Equation (A.4), it is remarkable that in the Hamiltonian constraint and evolution equation, the same terms in K are suppressed while the same terms in $D_i V_j$ are generated. This demonstrates the close relationship between Andersson-Moncrief and De Turck method.

Appendix B. Regularization of first order gauge-fixing

Undertaking the same reasoning as in Section 4, it happens that Equation (25) behaves like $O(\Omega^{-1})$ at the AdS boundary. So after multiplication by Ω , it takes the regularized form :

$$\Omega[2\hat{N}^2\hat{\gamma}^{ij}\partial_i\partial_j\alpha + 2\partial_i\hat{\beta}^i\hat{\beta}^j\partial_j\alpha + 2\partial_i(\hat{N}^2\hat{\gamma}^{ij})\partial_j\alpha + 2\partial_i\hat{\beta}^i + (\hat{\beta}^k + \{\hat{N}^2\hat{\gamma}^{kl} + \hat{\beta}^k\hat{\beta}^l\}\partial_l\alpha)\hat{\gamma}^{ij}\partial_k\hat{\gamma}_{ij}] - 6\Omega_i[\hat{\beta}^i + (\hat{N}^2\hat{\gamma}^{ij} + \hat{\beta}^i\hat{\beta}^j)\partial_j\alpha] = 0. \quad (\text{B.1})$$

A suitable boundary condition is to require α to be zero at the AdS boundary.

As for Equation (26), it becomes :

$$-\Omega^2\hat{\gamma}^{kl}\partial_k\partial_l\xi^i - \hat{\gamma}^{kl}(\Omega\mathcal{L}_\xi\hat{\Gamma}_{kl}^i - \hat{\Gamma}_{kl}^m\partial_m\xi^i) - (\hat{\Gamma}_{kl}^i - \hat{\Gamma}_{kl}^i)(\Omega\mathcal{L}_\xi\hat{\gamma}^{kl} + 2\hat{\gamma}^{kl}\xi^m\partial_m\Omega) + \Omega\hat{V}^i = 0. \quad (\text{B.2})$$

A suitable boundary condition is to require ξ^i to be zero at the AdS boundary.

Appendix C. Regularization of $T_{\alpha\beta}^{CFT}$

In order to compute numerically $T_{\alpha\beta}^{CFT}$ by Equation (38), we need to use only regular, non-diverging quantities. First, let us introduce r_α the unit normal to hypersurfaces $r = cst$, its acceleration a_α , $q_{\alpha\beta}$ the metric induced by $g_{\alpha\beta}$ and $\Theta_{\alpha\beta}$ the corresponding extrinsic curvature

$$r_\alpha = \frac{\partial_\alpha r}{\sqrt{g^{\mu\nu}\partial_\mu r\partial_\nu r}}, \quad (\text{C.1})$$

$$a_\alpha = r^\mu\nabla_\mu r_\alpha, \quad (\text{C.2})$$

$$q_{\alpha\beta} = g_{\alpha\beta} - r_\alpha r_\beta, \quad (\text{C.3})$$

$$\Theta_{\alpha\beta} = -\nabla_\beta r_\alpha + a_\alpha r_\beta. \quad (\text{C.4})$$

Corresponding regularized quantities are then

$$\hat{r}_\alpha \equiv \Omega r_\alpha = \frac{\partial_\alpha r}{\sqrt{\hat{g}^{\mu\nu}\partial_\mu r\partial_\nu r}}, \quad (\text{C.5})$$

$$\hat{a}_\alpha \equiv \Omega a_\alpha = r^\mu[\partial_\mu(\Omega\hat{r}_\alpha) - \hat{\Gamma}_{\mu\alpha}^\nu\hat{r}_\nu - 2\hat{r}_\alpha\Omega_\mu], \quad (\text{C.6})$$

$$\hat{q}_{\alpha\beta} \equiv \Omega^2 q_{\alpha\beta} = \hat{g}_{\alpha\beta} - \hat{r}_\alpha\hat{r}_\beta, \quad (\text{C.7})$$

$$\hat{\Theta}_{\alpha\beta} \equiv \Omega^2 \Theta_{\alpha\beta} = -\partial_\beta(\Omega\hat{r}_\alpha) + \hat{\Gamma}_{\alpha\beta}^\mu\hat{r}_\mu + 2\hat{r}_\alpha\Omega_\beta + \hat{a}_\alpha\hat{r}_\beta, \quad (\text{C.8})$$

where $\hat{\Gamma}_{\alpha\beta}^\mu = \Omega\Gamma_{\alpha\beta}^\mu$. The Riemann tensor of $g_{\alpha\beta}$ can be regularized as follows

$$\hat{R}_{\alpha\beta\mu\nu} \equiv \Omega^4 R_{\alpha\beta\mu\nu} = \hat{g}_{\alpha\rho}(\Omega\partial_\mu\hat{\Gamma}_{\beta\nu}^\rho - \Omega\partial_\nu\hat{\Gamma}_{\beta\mu}^\rho - \hat{\Gamma}_{\beta\nu}^\rho\Omega_\mu + \hat{\Gamma}_{\beta\mu}^\rho\Omega_\nu) + \hat{g}_{\alpha\rho}(\hat{\Gamma}_{\sigma\mu}^\rho\hat{\Gamma}_{\beta\nu}^\sigma - \hat{\Gamma}_{\sigma\nu}^\rho\hat{\Gamma}_{\beta\mu}^\sigma), \quad (\text{C.9})$$

which allows us to recover the regularized Riemann tensor of $q_{\alpha\beta}$ via the Gauss relation [66]

$$\hat{\mathcal{R}}_{\alpha\beta\gamma\delta} \equiv \Omega^4 \mathcal{R}_{\alpha\beta\gamma\delta} = \hat{q}_\alpha^\mu \hat{q}_\beta^\nu \hat{q}_\gamma^\rho \hat{q}_\delta^\sigma \hat{R}_{\mu\nu\rho\sigma} + \hat{\Theta}_{\alpha\gamma} \hat{\Theta}_{\beta\delta} - \hat{\Theta}_{\alpha\delta} \hat{\Theta}_{\beta\gamma}. \quad (\text{C.10})$$

From this, it is straightforward to get the regularized Einstein tensor of $q_{\alpha\beta}$, $\hat{\mathcal{G}}_{\alpha\beta} = \Omega^2 \mathcal{G}_{\alpha\beta}$. The quasilocal stress energy is then given by

$$8\pi GT_{\alpha\beta}^{CFT} = \frac{1}{\Omega^2} \left(\hat{\Theta}_{\alpha\beta} - \hat{\Theta} \hat{q}_{\alpha\beta} - \frac{2}{L} \hat{q}_{\alpha\beta} + L \hat{\mathcal{G}}_{\alpha\beta} \right), \quad (\text{C.11})$$

where $\hat{\Theta} = \hat{q}^{\alpha\beta} \hat{\Theta}_{\alpha\beta}$. Even if not obvious at first sight, the parenthesis is $O(\Omega^3)$ near the AdS boundary. To compute this formula numerically, we first compute the parenthesis and check that it is zero to machine precision at $r = L$. To compute the division by Ω^2 (that vanishes at the boundary), we take advantage of the spectral representation provided by the Kadath library and perform the division in coefficient space. In essence one uses the non-local nature of the spectral representation. This operation brings some numerical errors that can be monitored (see Section 7).

Appendix D. Mass and angular momentum tests of Kerr-AdS

In this appendix, we test our numerical determination of both AMD and BK charges on the analytical Kerr-AdS metric. This allows us to probe our absolute numerical precision on mass and angular momentum for a large number of different resolutions. The Kerr-AdS metric expressed in conformal coordinates (Equation (30)) is :

$$\begin{aligned} ds^2 = & - \frac{\Delta - (1 - \rho^2)^4 \Delta_\theta a^2 \sin^2 \theta}{(1 - \rho^2)^2 \Sigma} dt^2 + \frac{4}{(1 - \rho^2)^2} \frac{(1 + \rho^2)^2 \Sigma}{\Delta} dr^2 \\ & + \frac{\Sigma}{(1 - \rho^2)^2 \Delta_\theta} d\theta^2 + \frac{\Delta_\theta (4r^2 + a^2 (1 - \rho^2)^2)^2 - \Delta a^2 \sin^2 \theta}{(1 - \rho^2)^2 \Sigma \Xi^2} d\varphi^2 \\ & - \frac{\Delta_\theta (1 - \rho^2)^2 (4r^2 + a^2 (1 - \rho^2)^2) - \Delta}{(1 - \rho^2)^2 \Sigma \Xi} 2a \sin^2 \theta dt d\varphi, \end{aligned} \quad (\text{D.1})$$

with

$$\Delta = (4r^2 + a^2 (1 - \rho^2)^2) (1 + \rho^2)^2 - 4mr (1 - \rho^2)^3, \quad (\text{D.2})$$

$$\Sigma = 4r^2 + (1 - \rho^2)^2 a^2 \cos^2 \theta, \quad (\text{D.3})$$

$$\Delta_\theta = 1 - \frac{a^2}{L^2} \cos^2 \theta, \quad (\text{D.4})$$

$$\Xi = 1 - \frac{a^2}{L^2}, \quad (\text{D.5})$$

where we choose m and a to be positive without loss of generality.

As explained in [80, 82], the parameters m and a are not the mass M and angular momentum J of the black hole, but are related to them via

$$M = \frac{m}{\Xi^2} \quad \text{and} \quad J = -\frac{am}{\Xi^2}. \quad (\text{D.6})$$

It is a strange but physical effect of Kerr-AdS : J and a have opposite sign*, because the frame dragging function $\omega = -g_{t\varphi}/g_{\varphi\varphi}$ is positive near the horizon but negative and finite at the AdS boundary, whereas in asymptotically flat spacetimes, ω is positive everywhere and goes to zero on the sphere at infinity.

Applying either the AMD or BK definitions for charge, a naive computation gives

$$Q_{\partial_t}[\Sigma_t] = \frac{m}{\Xi} \quad \text{and} \quad Q_{\partial_\varphi}[\Sigma_t] = J. \quad (\text{D.7})$$

The reason why $M \neq Q_{\partial_t}[\Sigma_t]$ is that the observer whose worldline is attached to ∂_t at the AdS boundary is not a zero angular-momentum observer (ZAMO). A boundary ZAMO has actually an angular velocity $\omega = -a/L^2$. This spoils the charge computation, and the correct mass is given by the charge attached to the ZAMO worldline

$$M = Q_{\partial_t + \omega \partial_\varphi}[\Sigma_t] = Q_{\partial_t}[\Sigma_t] + \omega J. \quad (\text{D.8})$$

In order to test our charge computation numerically, we select a Kerr-AdS configuration with $m/L = 1$ and $a/L^2 = 0.5$, whose analytical charges are $M^0/L = 16/9$ and $J^0/L^2 = -8/9$, and compute numerically both AMD and BK charges taking into account Equation (D.8). For this configuration, the horizon lies at $\sim 0.37L$, so we use only one domain describing $r \in [0.5, 1]L$ to avoid the coordinate singularity.

In Figure D1, we show the relative difference between analytical and numerical charges as a function of radial resolution. As the results seemed quite insensitive to angular resolution, we fixed it at 9 points per octant. It is clear on this plot that both AMD and BK charges converge exponentially to the analytical value up to $N_r = 37-41$, after which rounding errors start to increase. At fixed resolution, BK is less precise than AMD, because of a more involved regularization procedure (see Section Appendix C). Furthermore, our precision saturates at $\sim 10^{-6}\%$, so that our absolute precision is around $\sim 10^{-8}$ at a resolution of $37 \times 9 \times 9$. This is quite large for an analytical metric, but we can't do much better in double precision arithmetics, since we need to perform several spectral operations like second order derivatives, divisions in coefficient space and surface integration.

* For geons, we also observed that J and Ω have opposite signs, however in the results presented in this paper we changed the sign of J , as it seems common in the literature.

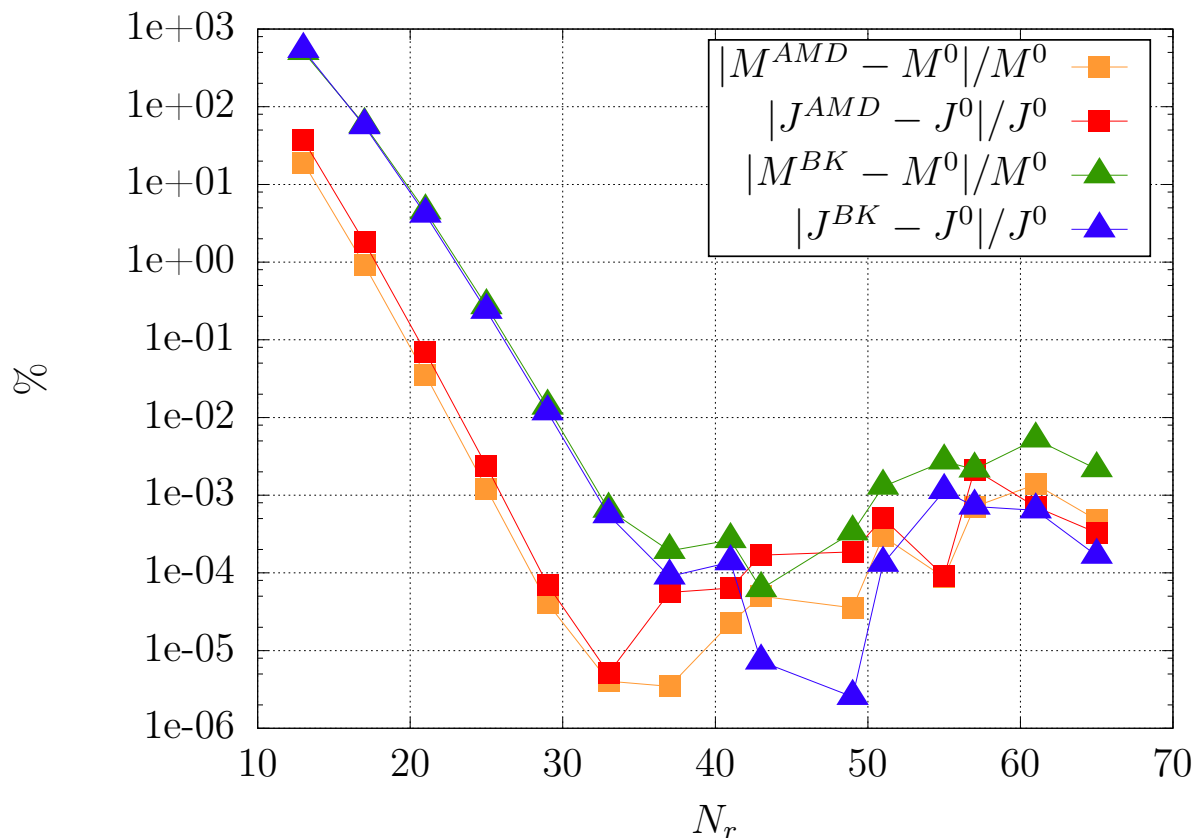


Figure D1. Relative differences between AMD, BK and analytical charges for the Kerr-AdS metric ($m/L = 1$, $a/L^2 = 1/2$) as a function of radial resolution. Angular resolution is fixed to $N_\theta = N_\varphi = 9$ assuming an octant symmetry.

References

- [1] J. M. Maldacena. The Large N Limit of Superconformal Field Theories and Supergravity. *Advances in Theoretical and Mathematical Physics*, 2:231, 1998.
- [2] E. Witten. Anti-de Sitter space and holography. *Advances in Theoretical and Mathematical Physics*, 2:253–291, 1998.
- [3] O. Aharony, S. S. Gubser, J. Maldacena, H. Ooguri, and Y. Oz. Large N field theories, string theory and gravity. *Phys. Rep.*, 323:183–386, January 2000.
- [4] V. E. Hubeny. The AdS/CFT correspondence. *Classical and Quantum Gravity*, 32(12):124010, June 2015.
- [5] P. Bizoń and A. Rostworowski. Weakly Turbulent Instability of Anti-de Sitter Spacetime. *Physical Review Letters*, 107(3):031102, July 2011.
- [6] J. Jałmużna, A. Rostworowski, and P. Bizoń. AdS collapse of a scalar field in higher dimensions. *Phys. Rev. D*, 84(8):085021, October 2011.
- [7] A. Buchel, L. Lehner, and S. L. Liebling. Scalar collapse in AdS spacetimes. *Phys. Rev. D*, 86(12):123011, December 2012.
- [8] M. Maliborski. Instability of Flat Space Enclosed in a Cavity. *Physical Review Letters*, 109(22):221101, November 2012.
- [9] P. Bizoń. Is AdS stable? *General Relativity and Gravitation*, 46:1724, May 2014.
- [10] M. Maliborski and A. Rostworowski. What drives AdS spacetime unstable? *Phys. Rev. D*, 89(12):124006, June 2014.

- [11] H. Friedrich. On the AdS stability problem. *Classical and Quantum Gravity*, 31(10):105001, May 2014.
- [12] P. Bizoń, M. Maliborski, and A. Rostworowski. Resonant Dynamics and the Instability of Anti-de Sitter Spacetime. *Physical Review Letters*, 115(8):081103, August 2015.
- [13] A. Buchel, S. R. Green, L. Lehner, and S. L. Liebling. Conserved quantities and dual turbulent cascades in anti-de Sitter spacetime. *Phys. Rev. D*, 91(6):064026, March 2015.
- [14] N. Deppe, A. Kolly, A. Frey, and G. Kunstatter. Stability of Anti-de Sitter Space in Einstein-Gauss-Bonnet Gravity. *Physical Review Letters*, 114(7):071102, February 2015.
- [15] B. Craps, O. Evnin, and J. Vanhoof. Renormalization group, secular term resummation and AdS (in)stability. *Journal of High Energy Physics*, 10:48, October 2014.
- [16] B. Craps, O. Evnin, and J. Vanhoof. Renormalization, averaging, conservation laws and AdS (in)stability. *Journal of High Energy Physics*, 1:108, January 2015.
- [17] O. Evnin and C. Krishnan. A hidden symmetry of AdS resonances. *Phys. Rev. D*, 91(12):126010, June 2015.
- [18] N. Deppe, A. Kolly, A. R. Frey, and G. Kunstatter. Black hole formation in AdS Einstein-Gauss-Bonnet gravity. *Journal of High Energy Physics*, 10:87, October 2016.
- [19] Umut Gürsoy, Aron Jansen, and Wilke van der Schee. New dynamical instability in asymptotically anti-de sitter spacetime. *Phys. Rev. D*, 94:061901, Sep 2016.
- [20] D. Santos-Oliván and C. F. Sopuerta. New Features of Gravitational Collapse in Anti-de Sitter Spacetimes. *Physical Review Letters*, 116(4):041101, January 2016.
- [21] D. Santos-Oliván and C. F. Sopuerta. Moving closer to the collapse of a massless scalar field in spherically symmetric anti-de Sitter spacetimes. *Phys. Rev. D*, 93(10):104002, May 2016.
- [22] R. Brito, V. Cardoso, and J. V. Rocha. Interacting shells in AdS spacetime and chaos. *Phys. Rev. D*, 94(2):024003, July 2016.
- [23] D. S. Menon and V. Suneeta. Necessary conditions for an AdS-type instability. *Phys. Rev. D*, 93(2):024044, January 2016.
- [24] O. Evnin and R. Nivesvivat. AdS perturbations, isometries, selection rules and the Higgs oscillator. *Journal of High Energy Physics*, 1:151, January 2016.
- [25] F. V. Dimitrakopoulos, B. Freivogel, J. F. Pedraza, and I.-S. Yang. Gauge dependence of the AdS instability problem. *Phys. Rev. D*, 94(12):124008, December 2016.
- [26] F. V. Dimitrakopoulos, B. Freivogel, and J. F. Pedraza. Fast and Slow Coherent Cascades in Anti-de Sitter Spacetime, arXiv 1612.04758. *ArXiv e-prints*, December 2016.
- [27] M. Maliborski and A. Rostworowski. Time-Periodic Solutions in an Einstein AdS-Massless-Scalar-Field System. *Physical Review Letters*, 111(5):051102, August 2013.
- [28] G. Fodor, P. Forgács, and P. Grandclément. Scalar field breathers on anti-de Sitter background. *Phys. Rev. D*, 89(6):065027, March 2014.
- [29] G. Fodor, P. Forgács, and P. Grandclément. Self-gravitating scalar breathers with a negative cosmological constant. *Phys. Rev. D*, 92(2):025036, July 2015.
- [30] H. Arodz, P. Klimas, and T. Tyranowski. Scaling, self-similar solutions and shock waves for V-shaped field potentials. *Phys.Rev. E*, 73:046609, March 2006.
- [31] H. Arodz, P. Klimas, and T. Tyranowski. Compact oscillons in the signum-Gordon model. *Phys. Rev. D*, 77:047701, 2008.
- [32] V. A. Koutvitsky and E. M. Maslov. Instability of coherent states of a real scalar field. *J. Math. Phys.*, 47:022302, 2006.
- [33] I. L. Bogolyubskii and V. G. Makhan'kov. Dynamics of spherically symmetric pulsions of large amplitudes. *JETP Letters*, 25:107, 1977.
- [34] M. Gleiser. Pseudostable Bubbles. *Phys. Rev. D*, 49:2978, 1994.
- [35] E. J. Copeland, M. Gleiser, and H.-R. Müller. Oscillons: Resonant configurations during bubble collapse. *Phys. Rev. D*, 52:1920, 1995.
- [36] E. P. Honda and M. W. Choptuik. Fine structure of oscillons in the spherically symmetric ϕ^4 Klein-Gordon model. *Phys. Rev. D*, 65:084037, 2002.

- [37] G. Fodor, P. Forgács, P. Grandclément, and I. Rácz. Oscillons and Quasi-breathers in the ϕ^4 Klein-Gordon model. *Phys. Rev. D*, 74:124003, 2006.
- [38] G. Fodor, P. Forgács, Z. Horváth, and Á. Lukács. Small amplitude quasibreathers and oscillons. *Phys. Rev. D*, 78:025003, 2008.
- [39] Segur H. and Kruskal M. D. Nonexistence of Small Amplitude Breather Solutions in ϕ^4 Theory. *Phys. Rev. Lett.*, 58:747, 1987.
- [40] G. Fodor, P. Forgács, Z. Horváth, and M. Mezei. Computation of the radiation amplitude of oscillons. *Phys. Rev. D*, 79:065002, 2009.
- [41] G. Fodor, P. Forgács, Z. Horváth, and M. Mezei. Radiation of scalar oscillons in 2 and 3 dimensions. *Physics Letters B*, 674:319, 2009.
- [42] Seidel E. and Suen W. M. Oscillating Soliton Stars. *Phys. Rev. Lett.*, 66:1659, 1991.
- [43] Seidel E. and Suen W. M. Formation of solitonic stars through gravitational cooling. *Phys. Rev. Lett.*, 72:2516, 1994.
- [44] D. N. Page. Classical and quantum decay of oscillations: Oscillating self-gravitating real scalar field solitons. *Phys. Rev. D*, 70:023002, 2004.
- [45] G. Fodor, P. Forgács, and M. Mezei. Boson stars and oscillatons in an inflationary universe. *Phys. Rev. D*, 82:044043, 2010.
- [46] P. Grandclément, G. Fodor, and P. Forgács. Numerical simulation of oscillatons: Extracting the radiating tail. *Phys. Rev. D*, 84:065037, 2011.
- [47] J. A. Wheeler. Geons. *Physical Review*, 97:511–536, January 1955.
- [48] D. R. Brill and J. B. Hartle. Method of the Self-Consistent Field in General Relativity and its Application to the Gravitational Geon. *Physical Review*, 135:271–278, July 1964.
- [49] P. R. Anderson and D. R. Brill. Gravitational geons revisited. *Phys. Rev. D*, 56:4824–4833, October 1997.
- [50] G. W. Gibbons and J. M. Stewart. Absence of asymptotically flat solutions of Einstein’s equations which are periodic and empty near infinity. In W. B. Bonnor, J. N. Islam, and M. A. H. MacCallum, editors, *Classical General Relativity*, pages 77–94, 1984.
- [51] A. Buchel, S. L. Liebling, and L. Lehner. Boson stars in AdS spacetime. *Phys. Rev. D*, 87(12):123006, June 2013.
- [52] S. R. Green, A. Maillard, L. Lehner, and S. L. Liebling. Islands of stability and recurrence times in AdS. *Phys. Rev. D*, 92(8):084001, October 2015.
- [53] N. Deppe and A. R. Frey. Classes of stable initial data for massless and massive scalars in Anti-de Sitter spacetime. *Journal of High Energy Physics*, 12:4, December 2015.
- [54] M. Duarte and R. Brito. Asymptotically anti-de Sitter Proca stars. *Phys. Rev. D*, 94(6):064055, September 2016.
- [55] C. Herdeiro and E. Radu. Einstein-Maxwell-Anti-de-Sitter spinning solitons. *Physics Letters B*, 757:268–274, June 2016.
- [56] Ó. J. C. Dias, G. T. Horowitz, and J. E. Santos. Gravitational turbulent instability of anti-de Sitter space. *Classical and Quantum Gravity*, 29(19):194002, October 2012.
- [57] Ó. J. C. Dias and J. E. Santos. AdS nonlinear instability: moving beyond spherical symmetry. *Classical and Quantum Gravity*, 33(23):23LT01, December 2016.
- [58] A. Rostworowski. Comment on ”AdS nonlinear instability: moving beyond spherical symmetry” [Class. Quantum Grav. 33 23LT01 (2016)] arXiv:1612.00042 [hep-th]. *ArXiv e-prints*, November 2016.
- [59] A. Rostworowski. Higher order perturbations of Anti-de Sitter space and time-periodic solutions of vacuum Einstein equations arXiv:1701.07804 [gr-qc]. *ArXiv e-prints*, January 2017.
- [60] Gary T. Horowitz and Jorge E. Santos. Geons and the Instability of Anti-de Sitter Spacetime. *Surveys Diff. Geom.*, 20:321–335, 2015.
- [61] H. Kodama, A. Ishibashi, and O. Seto. Brane world cosmology: Gauge-invariant formalism for perturbation. *Phys. Rev. D*, 62(6):064022, September 2000.
- [62] H. Kodama and A. Ishibashi. A Master Equation for Gravitational Perturbations of Maximally

- Symmetric Black Holes in Higher Dimensions. *Progress of Theoretical Physics*, 110:701–722, October 2003.
- [63] H. Kodama and A. Ishibashi. Master Equations for Perturbations of Generalized Static Black Holes with Charge in Higher Dimensions. *Progress of Theoretical Physics*, 111:29–73, January 2004.
- [64] A. Ishibashi and R. M. Wald. Dynamics in non-globally-hyperbolic static spacetimes: III. Anti-de Sitter spacetime. *Classical and Quantum Gravity*, 21:2981–3013, June 2004.
- [65] L. Andersson and V. Moncrief. Elliptic-hyperbolic systems and the einstein equations. *Annales Henri Poincaré*, 4(1):1–34, 2003.
- [66] Ericourgoulhon. *3+1 formalism in general relativity: bases of numerical relativity*, volume 846. Springer Science & Business Media, 2012.
- [67] P. Grandclément. KADATH: A spectral solver for theoretical physics. *Journal of Computational Physics*, 229:3334–3357, May 2010.
- [68] A. Ashtekar and A. Magnon. Asymptotically anti-de Sitter space-times. *Classical and Quantum Gravity*, 1:L39–L44, July 1984.
- [69] A. Ashtekar and S. Das. Asymptotically anti-de Sitter spacetimes: conserved quantities. *Classical and Quantum Gravity*, 17:L17–L30, January 2000.
- [70] V. Balasubramanian and P. Kraus. A Stress Tensor for Anti-de Sitter Gravity. *Communications in Mathematical Physics*, 208:413–428, 1999.
- [71] Dennis M. DeTurck. Deforming metrics in the direction of their ricci tensors. *J. Differential Geom.*, 18(1):157–162, 1983.
- [72] M. Headrick, S. Kitchen, and T. Wiseman. A new approach to static numerical relativity and its application to Kaluza-Klein black holes. *Classical and Quantum Gravity*, 27(3):035002, February 2010.
- [73] P. Figueras, J. Lucietti, and T. Wiseman. Ricci solitons, Ricci flow and strongly coupled CFT in the Schwarzschild Unruh or Boulware vacua. *Classical and Quantum Gravity*, 28(21):215018, November 2011.
- [74] Ó. J. C. Dias, J. E. Santos, and B. Way. Numerical methods for finding stationary gravitational solutions. *Classical and Quantum Gravity*, 33(13):133001, July 2016.
- [75] S. Bonazzola, E.ourgoulhon, P. Grandclément, and J. Novak. Constrained scheme for the Einstein equations based on the Dirac gauge and spherical coordinates. *Phys. Rev. D*, 70(10):104007, November 2004.
- [76] O. Mišković and R. Olea. Topological regularization and self-duality in four-dimensional anti-deSitter gravity. *Phys. Rev. D*, 79(12):124020, June 2009.
- [77] K. Uryū, A. Tsokaros, and P. Grandclément. New code for equilibriums and quasiequilibrium initial data of compact objects. II. Convergence tests and comparisons of binary black hole initial data. *Phys. Rev. D*, 86(10):104001, November 2012.
- [78] P. Grandclément, C. Somé, and E.ourgoulhon. Models of rotating boson stars and geodesics around them: New type of orbits. *Phys. Rev. D*, 90(2):024068, July 2014.
- [79] J. L. Friedman, K. Uryū, and M. Shibata. Thermodynamics of binary black holes and neutron stars. *Phys. Rev. D*, 65(6):064035, March 2002.
- [80] G. W. Gibbons, M. J. Perry, and C. N. Pope. The first law of thermodynamics for Kerr anti-de Sitter black holes. *Classical and Quantum Gravity*, 22:1503–1526, May 2005.
- [81] M. Alcubierre. *Introduction to 3+1 Numerical Relativity*. Oxford University Press, 2008.
- [82] M. M. Caldarelli, G. Cognola, and D. Klemm. Thermodynamics of Kerr-Newman-AdS black holes and conformal field theories. *Classical and Quantum Gravity*, 17:399–420, January 2000.